Chapter 5: Ambient Bubble Acoustics -Seep, Rain and Wave Noise

Ben Roche[1], Timothy G Leighton[1], Paul White[1], and Jonathan M Bull[1]

[1]University of Southampton

November 21, 2022

Abstract

This chapter discusses the sounds emitted by gas bubbles when they are generated underwater. Here we define bubbles to be volumes of gas, surrounded by liquid (here, taken to be water), having surface tension forces (the so-called Laplace pressure) generated by a single wall, and so are distinguished from the soap bubbles familiar in children's games, where the volume of gas is surrounded by two gas/liquid boundaries1. In comparison with other acoustic sources, such as marine mammals, ships and tectonic events, a single bubble may seem insignificant. Indeed, without ideal conditions it can be difficult to observe the sound of a single bubble from a distance of more than a few tens of centimetres. However, natural processes rarely produce single bubbles, and in fact can generate them in their millions at which point the sound generation is significant. With the formation of bubbles as a result of gas seeps, rainfall and breaking waves being a major component of ambient noise in the marine environment and can even alter the propagation of sound waves from other sources. This chapter focuses on the passive emissions of bubbles as they are formed, released, or injected into water, and here the volume pulsations are linear. In this chapter we will discuss the mechanics behind an individual bubble's acoustic signature, in particular the Minnaert equation and other relevant properties, before discussing the formation of bubbles from subsurface gas migration, rainfall and wave action, characterizing the acoustic nature of each process. The primary focus will be on the sound resulting from bubble generation from each of these sources. A number of different units are used to define each acoustic source, while this may appear confusing and make direct comparison difficult, this is done to be consistent with the literature. The topics covered here are broad, so the approach taken is to summarise the key principles and state of the field, while providing substantial linkage to the literature.

Hosted file

essoar.10512317.1.docx available at https://authorea.com/users/527814/articles/596721-chapter-5-ambient-bubble-acoustics-seep-rain-and-wave-noise

Noisy Oceans: Monitoring Seismic and Acoustic Signals in the Marine Environment

Chapter 5: Ambient Bubble Acoustics – Seep, Rain and Wave Noise

B. Roche, T.G Leighton, P. White, J.M. Bull

Contents

Chapter 5: Ambient Bubble Acoustics – Seep, Rain and Wave Noise ... 1
Bubbles as acoustic sources ... 3
The injection of a gas bubble ... 3
Bubbles as simple harmonic oscillators ... 5
Minnaert frequency ... 8
Subsurface gas release ... 13
Gas seep acoustics ... 15
Rainfall acoustics ... 19
Breaking wave acoustics ... 25
Conclusion ... 32
Further Reading ... 33
Appendix ... 34
Minnaert Frequency Derivation ... 34
Symbology ... 37
Bibliography ... 39

This chapter discusses the sounds emitted by gas bubbles when they are generated underwater. Here we define bubbles to be volumes of gas, surrounded by liquid (here, taken to be water), having surface tension forces (the so-called Laplace pressure) generated by a single wall, and so are distinguished from the soap bubbles familiar in children's games, where the volume of gas is surrounded by two gas/liquid boundaries[1]. In comparison with other acoustic sources, such as marine mammals, ships and tectonic events, a single bubble may seem insignificant. Indeed, without ideal conditions it can be difficult to observe the sound of a single bubble from a distance of more than a few tens of centimetres. However, natural processes rarely produce single bubbles, and in fact can generate them in their millions at which point the sound generation is significant. With the formation of bubbles as a result of gas seeps, rainfall and breaking waves being a major component of ambient noise in the marine environment and can even alter the propagation of sound waves from other sources. This chapter focuses on the passive emissions of bubbles as they are formed, released, or injected into water, and here the volume pulsations are linear.

In this chapter we will discuss the mechanics behind an individual bubble's acoustic signature, in particular the Minnaert equation and other relevant properties, before discussing the formation of bubbles from subsurface gas migration, rainfall and wave action, characterizing the acoustic nature of each process. The primary focus will be on the sound resulting from bubble generation from each of these sources. A number of different units are used to define each acoustic source, while this may appear confusing and make direct comparison difficult, this is done to be consistent with the literature. The topics covered here are broad, so the approach taken is to summarise the key principles and state of the field, while providing substantial linkage to the literature.

Bubbles as acoustic sources

While bubbles may be found throughout the water column and produced in all manner of ways, from fish flatulence to volcanic emissions, it is only the initial formation of the bubble near the source that is of interest in passive acoustics. Additionally, only a few sources of bubble production are common and large enough to warrant a full discussion, namely bubbles released from gas seeps on the seabed and those produced by either rainfall or breaking waves at the surface. The following section will discuss the initial release of gas bubbles into a body of water and the resulting acoustic signal. These are the fundamental principles behind bubble acoustics and are directly applicable to all initial sources of bubble production.

The injection of a gas bubble

A bubble does not instantly appear fully formed in the water column. The gas is injected into the body of water over a very short period of time. While there are several processes by which this injection can happen, the core principles remain the same; a small volume of gas from a larger reservoir encroaches into a body of water with the two volumes of gas being connected via a thin neck. As the small volume of gas extends further and further into the body of water the neck is stretched thinner and thinner, eventually snapping, and releasing the small volume of gas into the water as a distinct bubble. It is the snapping of the bubble neck that is of most interest to us as it results in a jet of water being momentarily propelled into the bubble, triggering an initial volume oscillation. This volume oscillation is ultimately what results in the acoustic signal of a bubble release [1–3].

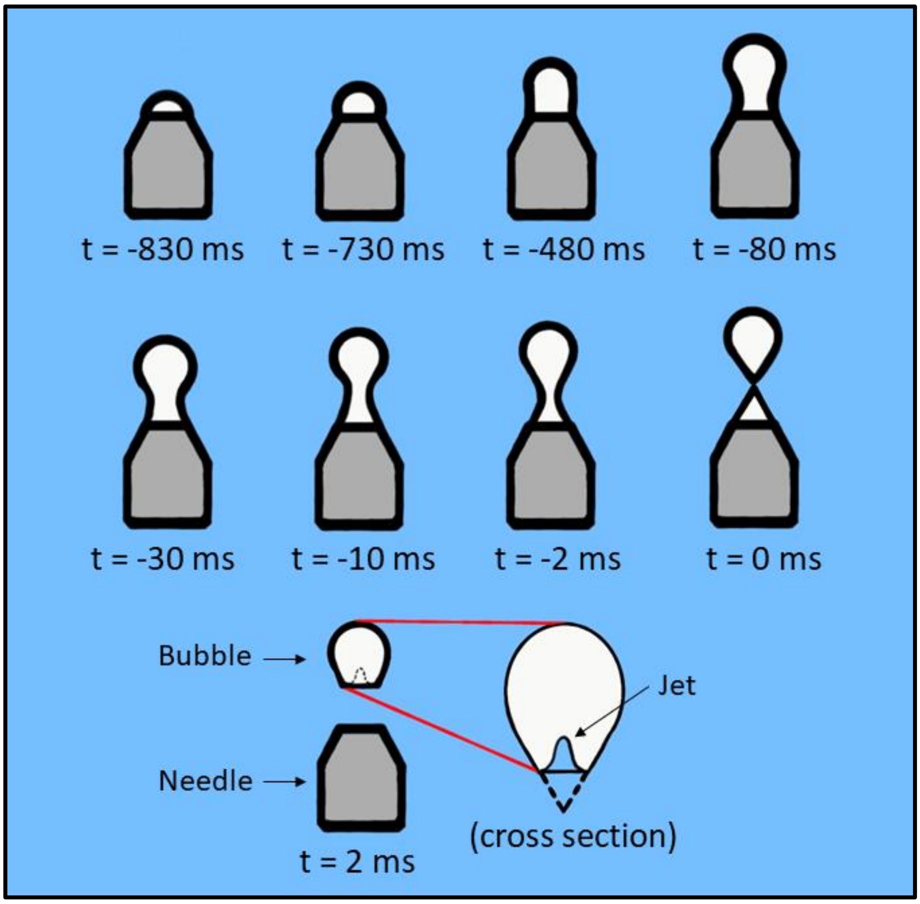

Figure 1; a bubble emerging from an underwater nozzle of internal diameter 4.00 mm. As the bubble grows a neck forms between it and the injection nozzle, the neck eventually snaps releasing the bubble and propelling a jet of water into the it. This jet decreases the volume of the bubble and causes it to undergo simple harmonic motion. Times are given in milliseconds relative to the moment the bubble is detached (i.e., the neck snaps), note these timings will change with nozzle size and gas flow rate. Adapted from Longuet-Higgins et al., 1991 and Czerski & Deane et al., 2010.

The easiest way to understand the process of bubble release is to study gas being injected into a body of water via a needle, as seen in figure 1. Theoretical calculations have been used to deduce the stages of bubble injection via a needle, reinforced by lab observations[2]. These stages are best described in relation to the radius of curvature (the radius of a circular arc that best approximates the curve) of the meniscus at the top of the bubble, the scales are dimensionless. The bubble initially grows from the surface of the nozzle as gas flows through it, the radius of curvature decreasing from 1 to <0.5 with volume increasing steadily (t = -830 ms in figure 1). The bubble profile changes from near horizontal to semi-circular in shape. Near the moment *the tangent to the meniscus at the point of attachment to the nozzle* becomes vertical (t = -730 ms in figure 1), the volume increases rapidly while the radius of curvature remains roughly constant (t = -480 ms in figure 1). Subsequently the volume and radius of curvature increase steadily. Here a "neck" begins to form, this is the narrowest part of the bubble profile, located between the nozzle and the main body of the bubble (t = -80 ms in figure 1). Once the radius of curvature equals ~0.655 the *tangent to the meniscus at the point of attachment* (now the neck of the bubble) becomes near vertical again and there is a second sharp increase in volume. The bubble now has a distinct diapir like shape (t = -2 ms in figure 1). The volume of gas in the bubble reaches a maximum, beyond this point the bubble in considered unstable. Further air forced into the bubble causes it to detach, a snapping of the neck releases the bubble allowing it to rise upwards (t = 0 ms in figure 1).[2] The upper half of the neck recedes back into the bubble as a jet of water propels itself inwards (t = 2 ms cross section in figure 1), this decreases the volume of the bubble resulting in a volume oscillation[1–3].

Bubbles as simple harmonic oscillators

Immediately after its release into the water column, regardless of the means of production, a bubble begins to pulsate. The bubble itself might undergo a wide range of oscillatory changes in shape, but these can be decomposed into a summation of spherical harmonic pulsations, and only one of these (the zeroth order) changes bubble volume to first order, and hence changes the gas pressure to first order (at low Mach numbers), and so couples to acoustic fields[1]. Therefore, despite the fact that the bubble will often depart from sphericity, with a few notable exceptions that will not be discussed further in this chapter[4], it is appropriate when discussing the interaction with sound fields at low Mach numbers to refer to the pulsations of a spherical bubble. This oscillation approximates a simple harmonic oscillator at low amplitudes, occurring at the natural frequency of the bubble[1]. It is possible to derive the relationship between the radius of a bubble and the frequency of its initial free oscillations by assuming there are no dissipative losses, e.g., through viscosity or thermal conduction, via consideration of the flow between potential and internal energy. The natural frequency of bubble oscillation is known the "Minnaert frequency"[5].

As a simple harmonic oscillator, the pulsation of a bubble is analogous to the classic bob on a spring system, of unloaded length l_0 and loaded length l. The water around the bubble are the bob weight and the gas within the bubble is the spring, as demonstrated in Figure 2a. Note that the contribution of the water to the effective mass of the system declines with distance from the bubble wall so that the mass is in effect finite. The displacement ε from the equilibrium position corresponds to displacement of the bubble wall R_ε between its equilibrium radius R_0 (the bob at $l - l_0$) and its present radius R at any given moment (the bob at $l + \varepsilon - l_0$), see figure 2. The gas pressure following compression or expansion act to restore the bubble to its equilibrium position, so is analogous to the spring stiffness in the spring-bob example. However, it is important to note that the gas in the bubble is less dense than the surrounding medium (unlike the bob in air). So, while in the spring-bob system inertia and momentum are dominated by the bob it is the inertia of the water surrounding a bubble which dominates in the bubble system, the mass of the gas being negligible.

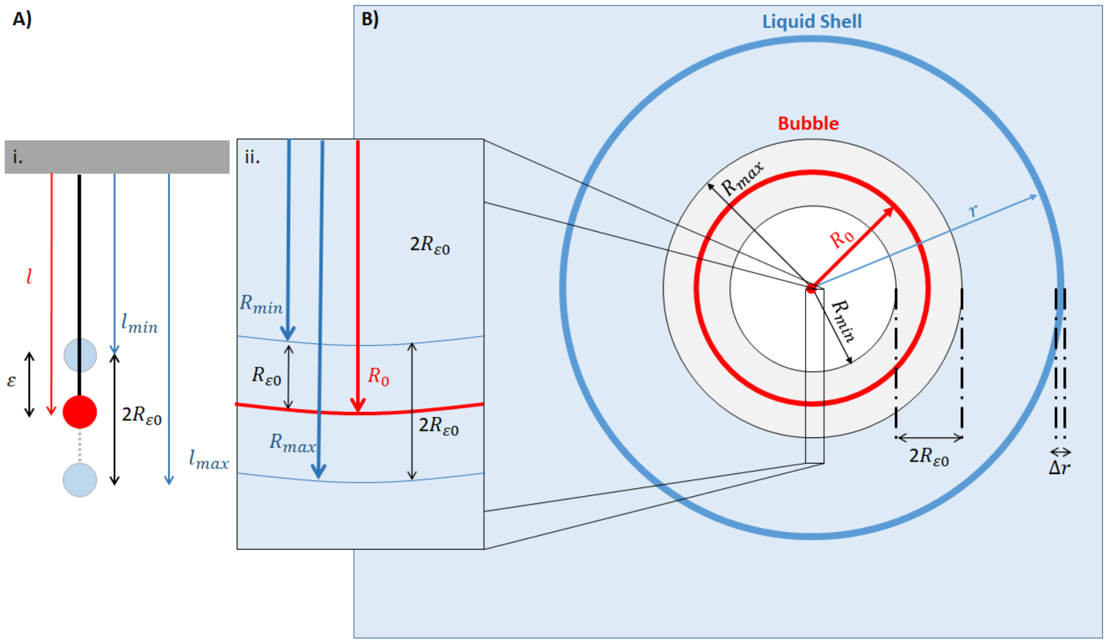

Figure 2; A) diagram comparing simple harmonic oscillators i. a spring bob system ii. a bubble wall moving B) diagram of a bubble of radius R_0 the wall of which is undergoing small amplitude oscillations of amplitude $R_{\varepsilon 0}$. It is surrounded by spherical shells of liquid, one of which has a radius of r and a thickness of Δr

It is this final stage of the bubble formation that triggers the simple harmonic motion of a bubble[1,3]. The snapping of the neck triggers an initial volume oscillation that acts as an exciting force causing the bubble to emit sound at its natural frequency. We assume this initial driving impulse is of an infinitesimally small duration meaning that while the bubble undergoes subsequent oscillation it effectively experiences no driving force.

With this idea of a bubble as a simple harmonic oscillator we can describe the shape of the bubble over time. Imagine a bubble (Figure 2b) with a mean radius of R_0 that remains spherical at all times while undergoing a volume oscillation at a frequency of ω_0. The maximum displacement of the bubble wall is $R_{\varepsilon 0}$ so that $R_{max} = R_0 + R_{\varepsilon 0}$ and $R_{min} = R_0 - R_{\varepsilon 0}$. Thus, the bubble radius R at any time t can be express as the real part of

$$R = R_0 + R_\varepsilon(t) = R_0 + R_{\varepsilon 0} e^{i\omega_0 t}. \tag{1}$$

The displacement of the bubble wall R_ε from equilibrium over time describes a motion

$$R_\varepsilon = -R_{\varepsilon 0} e^{i\omega_0 t}. \tag{2}$$

Minnaert frequency

With a description of the motion of the bubble wall over time we can describe the flow between kinetic and potential energy. From here we can apply the concept to conservation of energy in order to derive the Minnaert (or natural) frequency of a bubble[1,5].

$$f_M = \frac{1}{2\pi R_0}\sqrt{\frac{3\kappa p_0}{\rho}}, \tag{3}$$

ρ being the density of water, p_0 being the hydrostatic liquid pressure outside the bubble and κ being the polytropic index (which takes a value equal to unity when the gas behaves isothermally and equals the ratio of the specific heats of the gas at constant pressure to that at constant volume, when the gas behaves adiabatically). A full derivation of Minnaert frequency can be found in the appendix of this chapter.

The Minnaert equation demonstrates that the frequency of a bubble's oscillation is inversely proportional to its equilibrium radius R_0. As the other factors are fairly consistent or easily predictable (polytropic constant, density of water, water pressure outside of the bubble) it is relatively easy to measure the size of a bubble based on its acoustic signal. As a general rule of thumb for bubbles near the surface the radius in mm multiplied by the frequency in kHz is equal to approximately 3 i.e., a 1 mm radius bubble has a 3 kHz frequency, a 1.5 mm radius bubble has a 2 kHz frequency, and a 3 mm radius bubble has a frequency of 1 kHz

Once a bubble starts oscillating it begins to lose energy in three ways. Firstly (and most importantly for us) energy is radiated from the bubble through acoustic waves (radiation damping). Secondly energy is lost through conduction between the gas and the surrounding liquid (thermal damping). Finally energy is lost moving the water around the bubble as it oscillates (viscous damping)[1]. It is because of these factors that the bubble can be considered lightly damped[6]. This damping is typically described by the "quality factor" of the bubble, Q, which is approximately defined as the ratio of the initial energy to the energy lost in one radian cycle of oscillation[7]. We will avoid a full discussion on the damping constant of a bubble, see Ainslie and Leighton (2011) for this, and will note that the oscillation of millimetre sized bubbles decays exponentially over ~10-30 of milliseconds[1] and varies with gas content i.e., for air Bubbles $Q = 34$ while for pure methane bubbles and carbon dioxide bubbles $Q = 24$ and 29 respectively[7].

The polytropic adaptation of the Minnaert equation was first used in the 1980s to infer the size distribution and number of bubbles formed in the natural world, in waterfalls and streams[8], and over subsequent years this method was extended to do the same for bubbles entrained by breaking waves[9] and rainfall[10]. This method works well when the 'signature' passive emission from each bubble is clearly separated in time from others, however this method of counting and sizing bubbles becomes more difficult as the signatures from each bubble get closer in time and overlaps, and while signal processing techniques can alleviate the problem[11], eventually the degree of overlap becomes so great that this technique must be replaced by a spectral approach (discussed later)[12].

A recording of a bubble signature, as seen in figure 3, shows a sinusoidal wave which decays exponentially indicative of a lightly damped oscillator with a frequency consistent with that predicted by the Minnaert equation (equation 3). Though it should be noted that as the sound generated by a bubble is an exponentially decaying sinusoid, the sound will contain a range of frequencies and the spectral profile of each bubble will be Lorentzian[13], centred around the natural frequency[1]. The bubble seen in figure 3 was released at a water depth of 2.5 m has a frequency of 0.38 kHz. Using equation 3 (or the rule of thumb $R_{0(mm)} = 3/f_{M(kHz)}$) this corresponds to a radius of 7.9 mm.

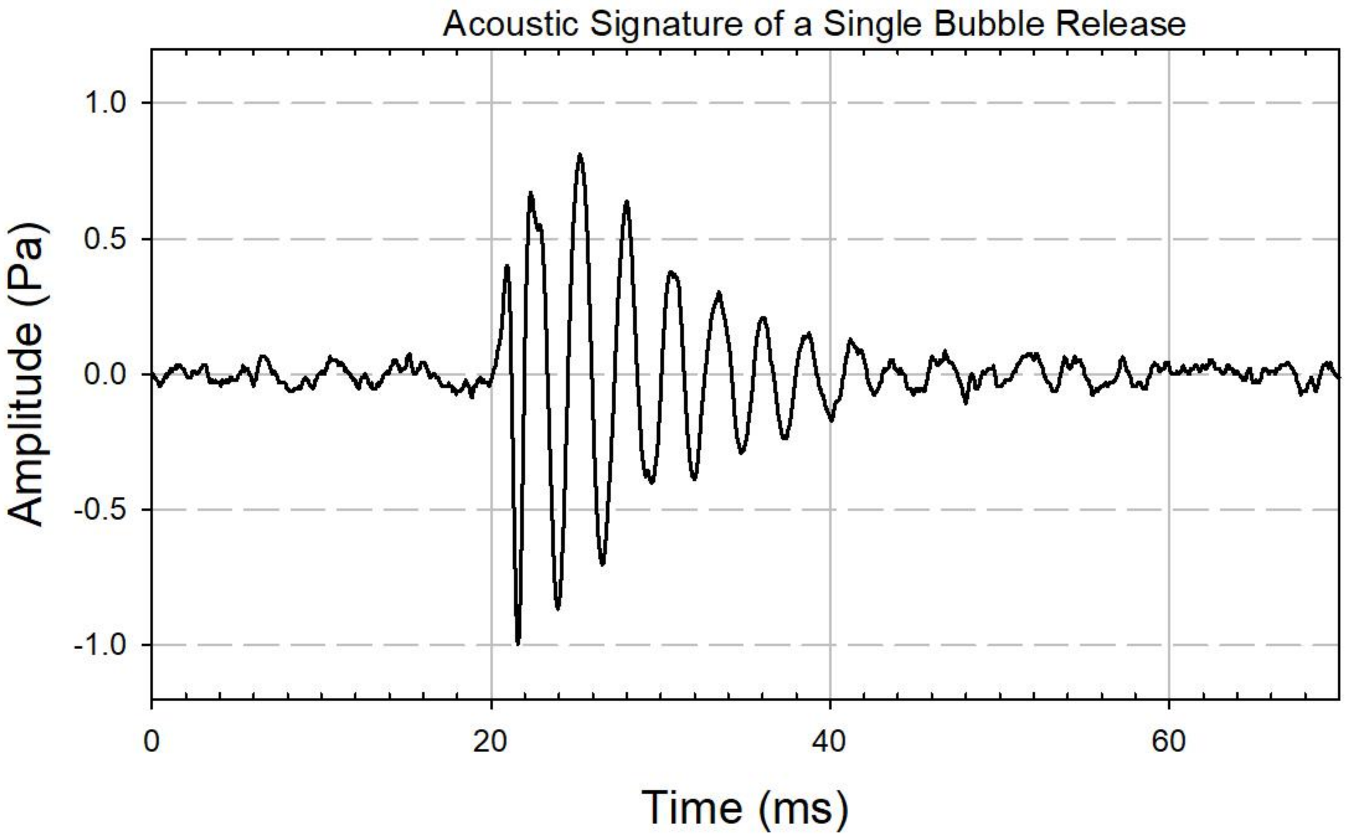

Figure 3; sonogram displaying the typical acoustic emission of a bubble as recorded by a hydrophone. Here the bubble was released from sediment at a water depth of 2.5 m, 25 cm from the hydrophone. The bubble became detached at around 20 ms, triggering simple harmonic oscillation resulting in exponentially decaying sinusoidal wave. The bubble oscillates with a frequency of 0.38 kHz (T = 2.6 ms) which we can inverted via the Minnaert equation (eq. 3) to indicate a radius of 7.9 mm.

The Minnaert equation was later adapted to include the effects of vapour pressure p_v, surface tension σ, and shear viscosity η and so is more correctly presented as[1,14];

$$f_M = \frac{1}{2\pi R_0\sqrt{\rho_0}}\sqrt{3\kappa\left(p_0 - p_v + \frac{2\sigma}{R_0}\right) - \frac{2\sigma}{R_0} + p_v - \frac{4\eta^2}{\rho_0 R_0^2}}, \tag{4}$$

Figure 4 displays the natural frequency of bubbles calculated using equation 4 at various sizes and depths.

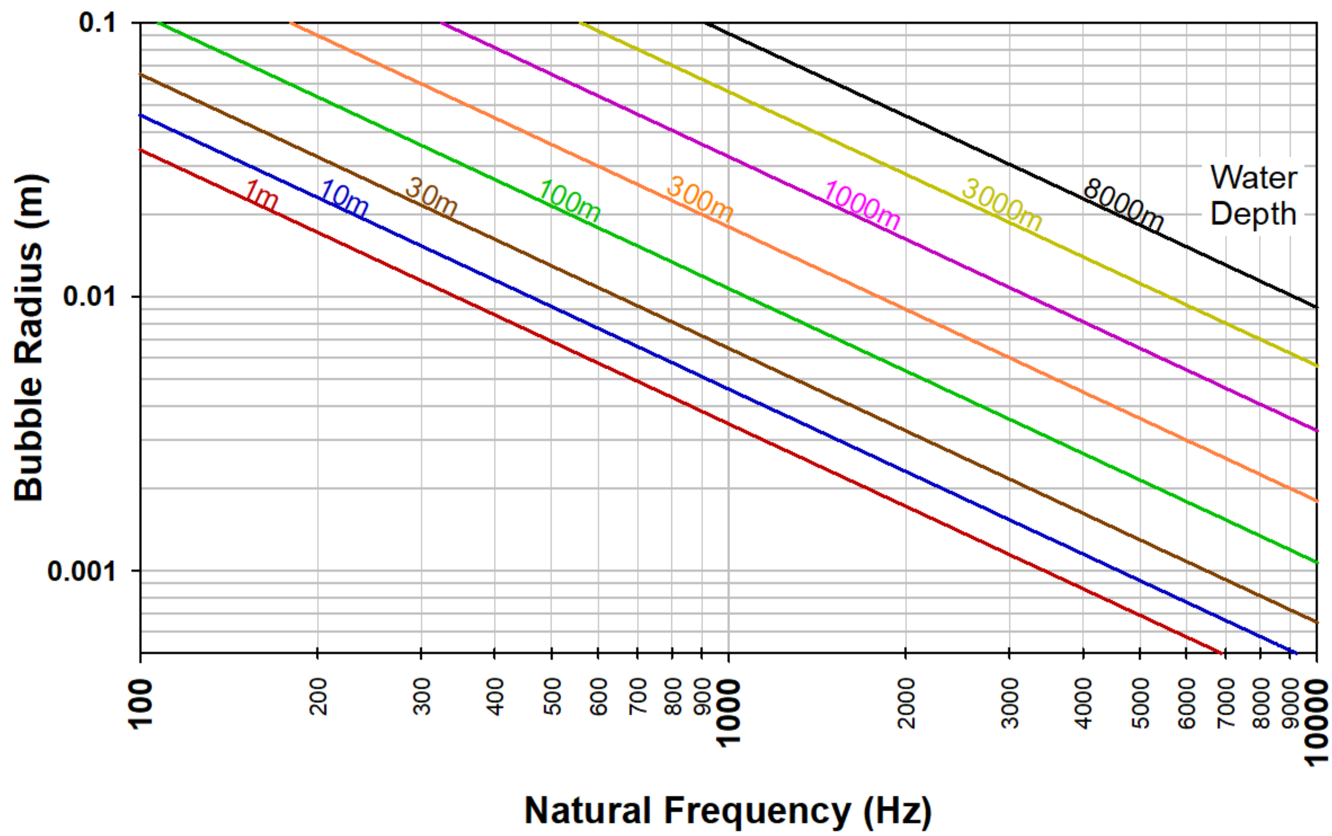

Figure 4; graph displaying the natural frequency of bubbles of various sizes according to the refined Minnaert equation (4) at a range of water depths 1, 10, 30, 100, 300, 1000, 3000 and 8000m. Calculated assuming ρ = 1000 kg/m^3, κ = 1.4, at a temperature of 10 °C and a salinity of 0 %.

Bubbles generated near the ocean surface will actually have a natural frequency f_0, which is slightly higher than that specified by the Minnaert equation as a consequence of the reduced inertia of the fluid near the surface. A similar effect occurs if the water surrounding the bubble also contains bubbles in close proximity. Strasberg calculated the effect on the frequency showing that[15].

$$f_0 = \frac{f_M}{\sqrt{1-\left({}^{R_0}/_{2h}\right)-\left({}^{R_0}/_{2h}\right)^4}}, \tag{5}$$

where h is the distance from the *centre* of the bubble to the surface of the water. As h is always greater than R_0, the denominator is always less than 1 and so, the oscillation of a bubble in the near surface is always slightly greater than that predicted by the Minnaert equation. For example, a bubble at a depth $h = 4R_0$ will have a frequency ~7% higher. Alternatively, one should also be able to see that when $h \gg R_0$, i.e., the bubble is a few tens of centimetres or more beneath the water's surface, the frequency of a bubble is equal to the Minnaert frequency.

$$f_0 = f_M \text{ for } h \gg R_0.$$

(6)

Another notable deviation from the Minnaert equation occurs when bubbles are generated (nearly) simultaneously in close proximity, as is the case with wave generated bubbles. The bubbles are linked by acoustic and hydrodynamic interactions resulting in coupled oscillator systems that tend to oscillate at much lower frequencies than the natural frequency of any individual bubble within it. In effect, a cloud of small bubbles can emit an acoustic signature similar to that of a much larger bubble. A region of bubbly water containing a total of N_b identical bubbles (each having a radius R_0 and a natural frequency of f_0) composes an air water mixture with a void fraction VF. If this bubbly water was submerged in bubble-free water and the boundary between the two were assumed to be rigid (a poor assumption but a useful starting point), then the modal frequency f_n of a bubble cloud can be given by[16]

$$f_n = f_0 \frac{n}{N_b^{1/3} \cdot \{VF\}^{1/6}},$$

(7)

where n is the mode of oscillation. It should be apparent that for any cloud with more than a few hundred bubbles the lower order modal frequencies will be lower than the natural frequency of the individual bubbles. E.g., a 10 cm cloud of 1000 bubbles will have a 1st order modal frequency 1/3 that of the bubble oscilations[1]. The greater the number of bubbles in the same space, the lower the modal frequency. Obviously, bubble clouds do not have rigid walls, but the general trend holds true with complexities in cloud geometry and bubble size distribution being a greater source of error. In practice this means that if bubbles exist in clouds, then the emission, and perhaps more prominently the scattering, of sound by the cloud of bubbles, will contain elements at this cloud frequency, in addition to the signals of the individual bubble resonances themselves[1].

In summary the release of a bubble into the water column causes it to undergo simple harmonic oscillation. The resulting acoustic signal is an exponentially decaying sinusoidal wave at the natural (or Minnaert) frequency of the bubble, which is approximately inversely proportional to its equilibrium radius. Measuring the volume of gas release at slow sources of bubble production (a few Hz) acoustically is relatively trivial. One simply

needs appropriate recording equipment and an understanding of the basic field/lab conditions (water depth etc.) to individually count and size each bubbles signal without needing any knowledge of the energy emission from an individual bubble[12]. Indeed this 'signature' method of flux measurement can even be used as an undergraduate lab experiment. However, as we will discuss later measuring the volume of released gas becomes increasingly difficult as the rate of bubble production increases.

Subsurface gas release

Gas can be generated below the seabed from a number of different sources namely thermogenic, biogenic, and anthropogenic. When this gas reaches the seabed, it will escape upwards into the water column by the formation of bubbles[17–19]. This can have a major impact on ocean chemistry via dissolution and is a poorly understood part of the global carbon cycle [20–23]. Additionally, the release of each bubble produces an acoustic signal which can affect soundscape in local areas [1,12,24]. The sound is emitted as soon the bubble detaches from the seafloor and lasts ~20 ms, which given that bubbles tend to rise upwards of a speed of 20-30 cm/s confines the production to within ~5 mm of the seafloor. We will first describe the passage and release of a single bubble before discussing localised seeps, their resultant signal and flux inversion techniques. The following is applicable to bubbles of any gas type, the Minnaert frequency varying only slightly as described by equation 4.

In a typical near-surface marine sediment, the pores between grains are saturated with water. The introduction of gas, for example from an underlying fault, slowly invades the surrounding pores, displacing the water. This intrusion can occur either by capillary invasion or by fracture opening[21–23]. The difference in density between the gas and the surrounding medium, creates a buoyancy force which typically causes the gas to rise upwards[25–27]. When gas reaches the seabed, it will continue to rise upwards due to the buoyancy forces. The sediment pores act like a kind of "nozzle", akin to a needle in a test tank, through which the bubble is injected into the water column[12,20]. The bubble will escape into the overlying water when the buoyancy forces acting on it overcome the adhesive like forces attaching it to the sediment.

The passage of gas through the upper few centimetres of the seabed can cause a weak oscillatory signal, audible in the water column, possibly as the grains rearrange to create an orifice for the bubble beneath the surface[1]. Vazquez et al., (2015) were able to observe this event using synchronous high-speed video and acoustic recordings of gas migrating through granular sediment[28]. The signal appears unpredictable and is expected to vary with grain size, grain type, bubble size, water pressure etc. Indeed, there is some experimental evidence indicating that the sound is absent for fine silts and coarse pebbles. As the magnitude of this precursor signal is smaller than that of subsequent bubble oscillation the phenomenon remains largely unexplored. Thus, the acoustic signature of a single bubble being released from sediment can be defined as an exponentially decaying sinusoidal wave resulting from bubble oscilation[8] potentially preceded by a weak unpredictable oscillatory signal in certain sediment types[28], as seen in figure 5.

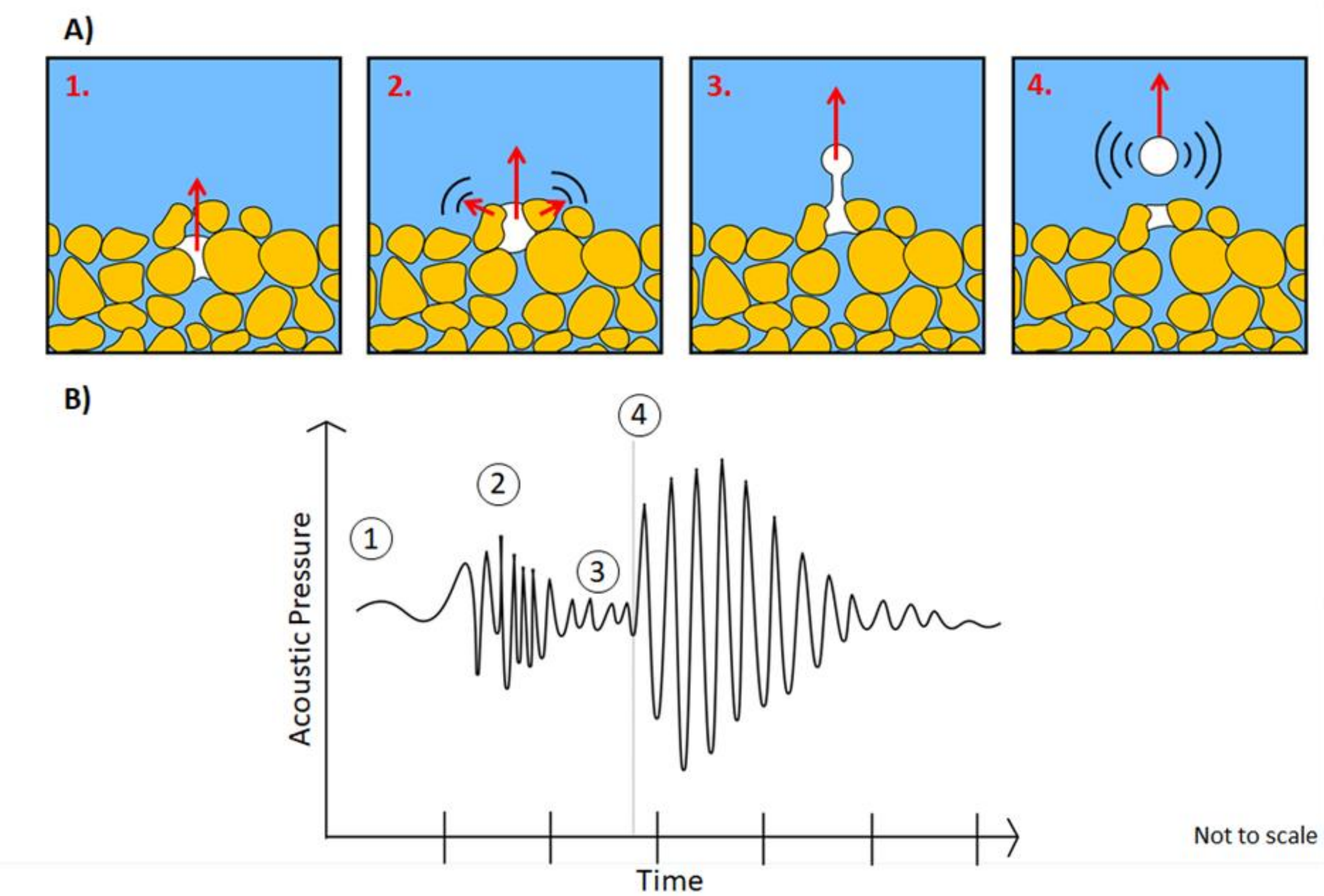

Figure 5 A) the release of a bubble from granular sediment and B) the corresponding acoustic signal. Note (2) the chaotic weak signal resulting from the rearrangement of grains as the gas reaches the seabed and (4) the stronger distinct acoustic signature of the bubble being released into the water column. Adapted from Vazquez et al., (2015)

Gas seep acoustics

The continuous passage of gas through the same area may cause the development of open channels (or chimneys) in the sediment which direct the flow of gas to a single localised point on the seabed, forming a seep[29–31]. A *subsea gas seep* is broadly defined by the *continuous* release of gas from the seabed into the water column. There is no set magnitude for the flux of gas from a seep[29–31], meaning the term encompasses seeps that release tens to millions of bubbles per minute. Similarly, there is no strictly defined time scales for being continuous, some seeps are born and die within a few hours, some are only active for certain times of the day or year while others have been active for centuries[30,32,33]. It is also worth noting a seep does not have to be in sediment, it may also come from exposed bedrock or even manmade features such as leaking pipes. The term pockmark is often synonymous with gas seep from sediment, though strictly speaking the term only defines the depressions created in the seabed by the gas release[30,33].

The size of a bubble released from the seabed is difficult to predict. In a lab the size of a bubble released from a needle is generally considered a factor of the size of the nozzle, the gas injection pressure, and the overlying water pressure, although even these have limited control of bubble size[2,34]. Even in a controlled setting it is difficult to regularly produce identically sized bubbles, making bubble size highly variable in the field. Assuming the pores between grains act as nozzles then one might anticipate that larger pore spacings, which are generally associated with the larger and more rounded the grains, would generate larger the bubbles. However, when open conduits form in sediment, pore size becomes less important in favour of conduit size which can vary significantly based on numerous factors including the age of the chimney. Consequently, bubble size distributions are unique for each seep, indeed the exact bubble size distribution (and thus gas flux) is likely to change over time as the underlying conduits evolve and the overlying water pressure fluctuates with tidal and seasonal variations[35–43]. Gas flux from underwater seeps can also vary as a result of underlying causes such as seabed temperature, seismic or volcanic activity[42,44–48]. In deep marine settings bubble sizes have commonly been observed between 1 and 6 mm in radius[36,49] while shallower waters (<10 m) have been observed to contain larger bubbles greater than 10 mm in radius[1,12,47,50], though this trend is far from a rule and exceptions are plentiful.

The acoustic signature of a seep is thus defined by its bubble generation rate i.e., the rate at which bubbles of different sizes are released. Unfortunately, as every seep has a unique bubble generation rate it is difficult to define a general rule for the passive acoustic emissions. In the simplest case of a “slow seep” releasing a few bubbles a second, its acoustic emission can be defined by the continuous release of bubbles, i.e., a continuous repetition of signal seen in figure 3[12,51]. Ultimately these signals are weak and have little impact on the marine soundscape due to the flux rates being so low meaning they are of little interest to many researchers.

Larger seeps with higher gas flux rates, generate stronger signals which can be observed at greater distances and may have a noticeable impact on ocean chemistry. However, as the frequency of bubble release increases with flux rate eventually the acoustic signals of each release begin to overlap making it impossible to distinguish individual bubble oscillations[36,52,53].

By considering the combined signal of multiple bubble releases Leighton and White (2012) derived the power spectral density $S(\omega)$ of the far field acoustic signature of a gas seep at some distance r;

$$S(\omega) = \int_0^\infty B(R_0)|X_b(\omega, R_0)|^2 \, dR_0, \tag{8}$$

where ω is the angular frequency, $B(R_0)$ is the bubble size distribution as a function of R_0 defined such that $\Psi(n) = \int_{R_1}^{R_2} B(R_0) dR_0$ represents the number of bubbles generated per second with a radius between R_1 and R_2 i.e., the bubble generation rate, δ_{tot} is the total damping constant for pulsation at resonance and

$$|X_b(\omega, R_0)|^2 = R_{\epsilon 0i}^2 \frac{\omega_0^4 R_0^4 \rho^2}{r^2} \left(\frac{4[(\omega_0 \delta_{tot})^2 + 4\omega^2]}{[(\omega_0 \delta_{tot})^2 + 4(\omega_0 - \omega)^2][(\omega_0 \delta_{tot})^2 + 4(\omega_0 + \omega)^2]} \right). \tag{9}$$

The important unknown in this equation is the initial amplitude of displacement of the bubble wall at the start of the emission ($R_{\epsilon 0i}$) [not to be confused with $R_{\varepsilon 0}$ the maximum displacement of bubble wall from the equilibrium radius]. There is strong evidence to suggest this is a function of the equilibrium bubble radius (R_0). However, this exact relationship is yet to be defined. Consequently, many studies have elected to treat $R_{\epsilon 0i}/R_0$ as a constant existing somewhere between 1.4×10^{-4} and 5.6×10^{-4}, based on experimental observations[12]. Though it should be stressed this is a pragmatic choice with no theoretical foundation. It is important to note that the above formulation excludes the signal from the rearrangement of grains prior to a bubbles release. However, this is reasonable as 1) the signal is very weak[28] and 2) seeps with a higher flux contain open conduits that do not require grains to be rearranged to facilitate the migration of gas[20].

This spectral approach allowed Leighton and White to invert the signal from a given gas seep (at a known distance from a hydrophone) to determine the number of bubbles of various sizes released within a given period, providing them with an estimate of gas flux [12]. In replacing the signature method for counting and sizing bubbles in circumstances where their passive acoustic emissions overlapped, they drew particular attention to the lack of knowledge about the energy of an individual bubbles' emission. While the signature method had managed to bypass this unknown their spectral method could not. Whilst the spectral method had the power to count and size bubbles when the signatures overlapped, they noted that the reliance on literature values for the energy released by a bubble was the greatest source of uncertainty, particularly as the energy associated with the release of a given bubble is likely to vary with the mode by which it is entrained (injected by a needle, or through sediment, via a gas pipe leak or entrained in the upper ocean by rainfall or breaking waves), and the depth at which it is entrained. In simple terms, if the count of bubbles of a certain size is based on the energy detected in a given frequency band, then if the acoustic energy in that band is divided between the bubbles contributing to it, the estimation calculates fewer bubbles were entrained the more acoustic energy is contained in each bubble signature[12]. Further complications were identified, in that a given injection process can cause the bubble to fragment after release, or merge with other bubbles, and this can lead to the injection of a single bubble generating multiple signatures[34]. Despite all of this, to date the use of the spectral method in the field has proven effective, providing continuous estimates of gas flux over extended periods of time validated by intermittent physical measurements. However, a need to reduce the uncertainty in these measurements is continually noted[36,50,52].

Given the highly variable nature of seafloor gas seeps, particularly in regard to the size of the bubbles and their rate of release, it is difficult to give a general impression of their contribution to the marine soundscape. In order to do so here we use the above equations to simulate the sound pressure level (SPL) of a single point focused seep venting gas at the rate of 10, 100, 1000 and 10,000 L/min assuming a log normal bubble size distribution between 0.5 and 10 mm radius. The results are displayed in figure 6 alongside the SPL of various intensities of wind and rain generated bubble noise. We would emphasise that these graphs are meant to serve only as an approximate guide to the potential effect natural seeps can have on the marine soundscape. Here we see the signal is confined mainly between 1 to 10 kHz (a result of the selected bubble size distribution) with the magnitude of the signal increasing in line with rate of gas flux. A maximum amplitude of 97 dB rel $1\mu Pa^2/Hz$ is seen at 10,000 L/min, well in excess of wind and rain generated bubble noise.

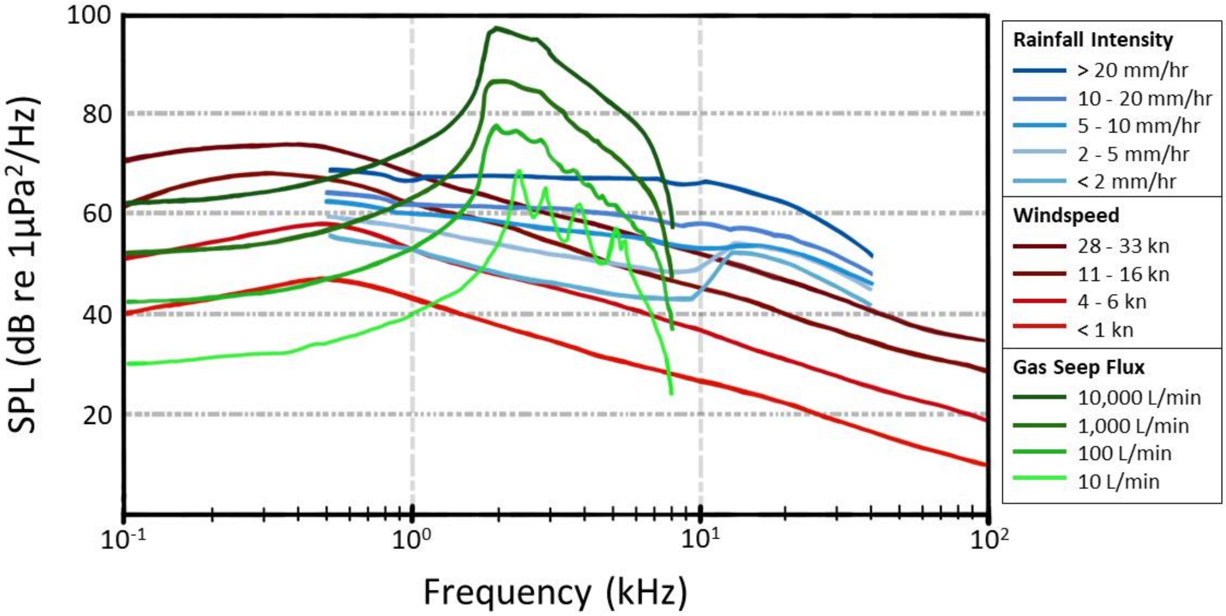

Figure 6; Ambient noise spectral density from 0.1 to 100 kHz for common bubble production sources in the marine environment including gas seeps, rainfall, and breaking waves. Gas seepage is simulated at different flux rates in *L/min* at 100 m water depth assuming a Gaussian bubble size distribution between *0.5 - 10 mm radius. Rainfall data at different intensity levels in mm/hr is from* Ma and Nystuen (2004), breaking wave data observations *at different wind speeds in knots is from* Wenz (1962).

In summary the release of gas from the seabed releases an acoustic signal at the natural frequency of the resulting bubble. As the flow of gas out of a seep increases the acoustic signals of each bubble released begins to overlap making the resultant signal a summation of each individual bubble's natural frequency. Consequently, it is currently impossible to predict the sound resulting from a gas seep (or indeed a field of seeps) without an understanding of its bubble size distribution. However, by observing the acoustic signature of a known seep, it is possible to quantify the size of bubbles being released and thus estimate the flux, observing tidal and seasonal variations.

Rainfall acoustics

When a rain droplet impacts a body of water it forms an impact crater and may entrain a bubble. Consequently, falling rain produces two sounds in the marine environment, figure 7a, firstly the initial impact of the droplet on the body of water which generates a compressional wave. Secondly the simple harmonic motion of a bubble following its release into the water, once again at the Minnaert frequency[1]. This scenario is directly comparable to a leaky tap dripping water into a sink, producing a distinct “plinking” noise[1,54,55]. While some incorrectly assume this sound is a consequence of the initial collision between drop and water surface, it is in fact the entrainment of bubbles that produces the majority of the acoustic signature. We will first discuss the sound of the initial droplet impact before discussing the processes of entrainment, the resulting acoustic signature of rainfall and methods of rainfall quantification.

The impact of the rain droplet on the water’s surface initially produces a sharp acoustic pulse, with a duration of 10-40 µs, as a result of the “water hammer” effect (a pressure surge caused when the motion of a fluid is stopped). The pressure radiated by the impact is given by[10].

$$p_{impact} = \frac{\rho u_d^3 L_d}{2c}\frac{\cos\theta}{r}\boldsymbol{u}, \tag{10}$$

where ρ is the water density, u_d is the impact speed of the droplet, L_d is the diameter of the droplet, c is the speed of sound in water, θ is the angle between the observer and sound source relative to the z axis, and $\boldsymbol{u}$ is the impact Mach number. Raindrops typically have a diameter between 0.5 to 5.0 mm (larger droplets tending to break up) resulting in an impact velocity between ~2.0 and 9.0 m/s[56]. This means that while for individual droplets it is easy to identify the impact signature, this sound is dwarfed by the later oscillation of a bubble, by a factor as large as 200:1, meaning that during rainfall (where bubbles are continuously oscillating) the sound of impact has very little effect on the overall acoustic signature, and is responsible only for a weak broadband signal[54].

The entrainment of a bubble by a droplet of water is dynamic process, much more complex than the injection of gas through sediment pores. The exact mechanism by which this occurs varies based on a number of factors, mainly impact velocity and droplet diameter. These processes are[54].

1) Irregular Entrainment: in which the complex and unpredictable details of a splash somehow entrain a bubble(s)

2) Regular Entrainment: in which a retreating impact crater leaves behind a small volume of gas connect via a narrow neck that is eventually pinched off leaving behind a single bubble (see figure 7a)

3) Entrainment of large bubbles: in which most of the volume of the crater is trapped as a bubble

4) Mesler Entrainment: in which many tiny bubbles are trapped in the early stages of impact process, possibly between the crest of capillary waves on the droplet and body of water

Bubbles produced by entrainment act identically to examples discussed previously, oscillating to produce an exponentially decaying sinusoidal wave in the near field[54]. The only notable difference to seabed gas release is that the bubbles are much closer to a free surface (the water surface), meaning the mass of water regulating the oscillations is lower and thus the natural frequency of the bubbles is slightly higher than the Minnaert frequency (see equation 5).

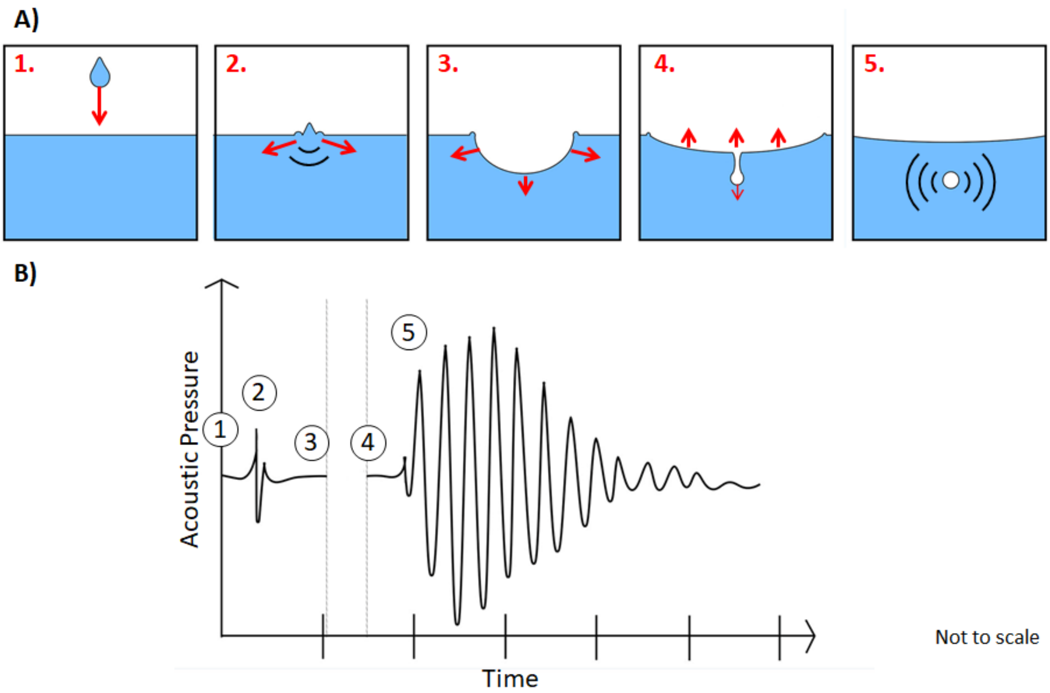

Figure 7; A) a diagram of regular entrainment of a bubble following the impact of a water droplet B) the acoustic signature of a raindrop. Note the weak sharp signal from the impact itself (2) followed by the larger oscillation of the bubble (5) once it detaches from the crater. Adapted from Medwin & Nystuen (1990)

Given a large enough area and a large enough number of raindrops (of a consistent size distribution), one can assume a constant number of raindrops are impacting the water per second and therefore a constant number of bubbles are being entrained. Consequently, rainfall results in a constant “ambient” noise. Using this principle and quantifying the number of bubbles entrained per second $n(f)$ in a 1 Hz frequency band over a 1 m^2 area of water, Pumphrey & Elmore (1990) were able to show that the intensity below the surface of the oscillating bubbles at any given frequency f is.

$$I_{Rain} = \frac{n(f)D^2Q}{4f\rho c}, \tag{11}$$

where Q is the quality factor and D is the initial dipole strength of the bubble. From which the intensity spectrum level is given by.

$$ISL_{Rain} = 10\log\frac{I_{Rain} \cdot \rho c}{1\ \mu Pa^2/Hz} = 10\log\frac{n(f)D^2Q/4f}{1\ \mu Pa^2/Hz}. \tag{12}$$

From here it is important to note that while D increases with increasing f, Q decreases. these two effects cancel each other out meaning the spectrum is dominated by the number of bubbles entrained per second[54]. Additionally, it has been observed that, neglecting refraction and absorption, 90% of the rain signal arrives from a sample area with a radius equal to 3 times the observer's depth[54]. Thus, using equation 12 and the size and number of bubbles produced per second by entrainment one can calculate the acoustic spectrum produced by rainfall or vice versa.

It is difficult to precisely predict the relative occurrence of each entrainment process during a rainstorm. While regular entrainment is by far the most well understood process, its name is more a consequence of being the easiest to comprehend and predict. Indeed, when Pumphrey and Elmore (1990) mapped which process occurs at which impact velocity to drop diameter ratio the plot is dominated by Mesler entrainment. Additionally, if one were to assume all impacts occurred at terminal velocity then the entrainment of large bubbles would never occur, and irregular entrainment would occur only during storms with particularly large droplets[54,56–66]. It is logical to assume that the splashing of water will produce some droplets that impact at below terminal velocity meaning all entrainment processes are likely to occur at some point during a rainstorm. However, it is reasonable for now to assume only regular and Mesler entrainment dominate and justify further consideration.

Mesler entrainment produces multiple very small bubbles ~25 µm in radius regardless of the size and velocity of the droplet. This results in a natural frequency of approximately 1.3 MHz. The high frequency / small size of Mesler bubbles ultimately means they produce very little noise with high levels of attenuation and consequently have little to no impact on the acoustic signature of rainfall, especially in the far field, meaning regular entrainment is responsible for the majority of bubble oscillation sound during rainfall[54,56–64,67–71].

Regular entrainment produces different bubble sizes for different droplet sizes and impact velocities. If we consider only the bubbles produced by raindrops traveling at terminal velocity, regular entrainment is the result of droplets 0.40 to 0.55 mm in radius (with larger and smaller droplets resulting in Mesler entrainment)[57,64,71]. Bubbles produced by regular entrainment of droplets of this size are predicted to be in the range 0.16 to 0.33 mm in radius, resulting in frequencies between 10 and 20 kHz. Laboratory and field data has consistently shown that there is a general increase in the number of bubbles entrained with bubble radius, peaking at ~0.23 mm in radius and dropping off rapidly above ~0.27 mm[54,57,61,64,66].

Consequently, the spectral content of rainfall on a body of water is expected to have a gradually increase in intensity with decreasing frequency, leading to a large peak at around 14-15 kHz and followed by a sharp decline below 10-12 kHz, the exact intensity of the signal depending on the number of bubbles entrained per second (a consequence of the number of raindrops impacting per second)[56,57,64]. This prediction fits well with field observation, see figure 8. Data collected from lakes, land-based water tanks, brackish ponds and deep marine environments all show a distinctive peak at 14-15 kHz with a sudden drop off below 10-12 kHz [56].

One consistent observation in repeat studies is a decrease in the prominence of the 14-15 kHz peak with increased rates of rainfall, with the peak being almost indistinguishable above 30 mm/hr as seen in figures 6 and 8[72,73]. This is because at higher rainfall rates, more bubbles oscillating between 10 to 20 kHz are generated per second resulting in an increased intensity of the signal. However as can be seen in equation 12 this is a logarithmic increase with diminishing returns meaning while the surrounding frequencies increase in intensity the 14-15 kHz peak is relatively unmoved, flattening out the spectrum. Additionally, in the field increased rainfall tends to be accompanied by increased windspeed, which as we will discuss next also affects the rain spectrum. For this reason, the rain spectrum is best observed during a drizzle or light rain[74].

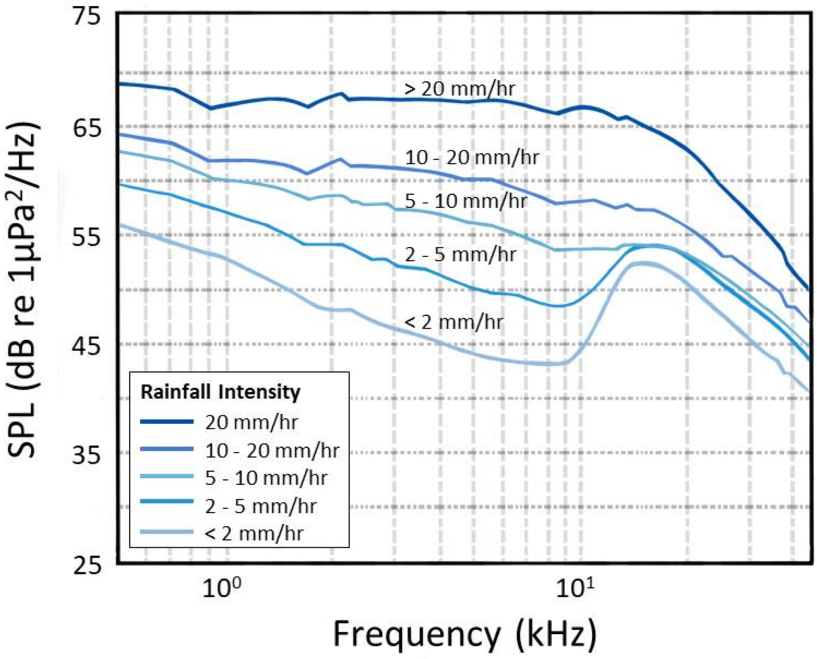

Figure 8; the average SPL spectra of rainfall acoustic at various rates as record by a number of buoys in lakes and seas around the world over a collective total of 30 months. Note the distinct peak at 14 kHz caused by the regular entertainment of bubbles from rainfall that becomes less prominent as rainfall become more intense. Adapted from Ma and Nystuen (2004).

The rain signature above 10 kHz is known to be affected by wind speed[54,57,58,65]. Ma and Nystuen (2004) noted that as wind speed increased from 0.6 to 3.3 m/s, the 15 kHz peak became less prominent and broader, shifting up by a few kHz. The increased wind speed drives waves on the surface of the water which has two effects. Firstly, it alters the angle of incidence of raindrops on the water, this reduces the probability that an individual droplet will produce a bubble from a 100% at normal incidence to 10% at a deviation of 20° [57]. Additionally, a deviation of 20° causes a 30% decrease in the energy emitted by the initial impact[57]. This means that dominance of the bubble noise over the impact noise reduces by a factor of 10, thus making the peak less prominent. Secondly, as we will discuss later, at high wind speeds breaking waves / white caps can also produce bubbles of similar magnitude which will interfere with the sound of rainfall. However, it has been observed that under certain conditions rainfall can prevent the formation of breaking waves [1,75–77].

Some studies have noted a secondary rise in the rain spectrum starting at 2-3 kHz and peaking around 5 kHz. This is believed to be a consequence of irregular entrainment of bubbles caused by very large droplets 2.0-3.5 mm in diameter [59–62,65]. We had previously dismissed irregular entrainment and the entrainment of large bubbles by assuming all the droplets impacted at terminal velocity and that larger droplets were less common than small ones. However, it appears that when a rainstorm is comprised of particularly large droplets (>2.0 mm) the frequency of irregular and large entrainment events is significant enough to cause a recognisable spike in the spectrum. Possibly as a result of accompanying wave action lowering the impact velocity. This secondary 5 kHz peak while less conspicuous than the 14-15 kHz peak may in fact be more useful as it exists in the part of the spectrum less affected by wind and wave noise (2 - 10 kHz)[57]. This means that observations of the intensity of the 5 kHz peak can be used for rainfall quantification regardless of windspeeds. Using comparative rain gauge data Ma and Nystuen (2001) proposed the following equation for calculating the rainfall rate S_{rain} in mm/hr based on the sound pressure level at 5 kHz (SPL_{5kHZ}).

$$10\log_{10} S_{rain}/10 = (SPL_{5kHZ} - 42.4)/15.4. \tag{13}$$

While the exact relationship varies from location to location based on local conditions and ambient noise levels, acoustic inversion of rainfall (with sufficient calibration) is a highly promising technique for use in meteorological & oceanographic research which is becoming increasingly common[57,60–62,65,71,73,78].

In summary the acoustic signature of rainfall in the marine environment is caused by the entrainment of bubbles, not the impact of the droplets themselves. The rain spectrum is a distinctive peak at 14-15 kHz with a sudden drop off below 10-12 kHz, caused by regular entrainment, and occasionally a secondary smaller peak at 5 k Hz, caused by irregular entrainment when droplet are particularly large. The intensity of these peaks is dictated by the number of raindrops impacting the water per second. As the intensity of the rainfall increases the peaks becomes broader and less well defined. Increasing wind speeds also mutes the 14-15 kHz peak due to altering the impact angle of droplets and interference from wave noise, however the 5 kHz peak is less affected by wind and can be used for rainfall quantification.

Breaking wave acoustics

In the natural marine environment sufficiently high wind speeds can cause surface gravity waves to break as whitecaps (or whitehorses)[1]. Unsurprisingly this process entrains a large number of bubbles which oscillate near the surface, as described by equation 5[78–81]. Not only do these bubbles have a noticeable effect on the ambient noise of the ocean (via oscillation)[78] but they may also affect the passage of other acoustic signals by altering the propagation of sound waves near the sea surface[78]. First, we will discuss waves as acoustic sources before discussing the effect wave generated bubbles have on the speed of sound and finally the ambient noise generated by wave action and how this can be related to wind speed. We will not discuss in detail the hydrodynamic controls behind breaking waves, other than to note, in general, strong winds result in larger breaking waves, as this in itself would demand a full chapter[1,78].

The entrainment of bubbles from wave action is a highly dynamic process (even more so than rainfall) with the exact minutia of the bubble generation being poorly understood[78]. We know, however, from laboratory and field data that distinct bubbles are initially generated during one of two phases: Jet Entrainment and Cavity collapse[78].

Jet entrainment begins as soon as the wave starts to break. The crest of the wave overturns and plunges into the wave face, forming a plunging jet, with a cavity of air trapped between the two bodies of water. This chaotic collision of the jet generates bubbles generally between 0.1 and 2.0 mm in radius (2 to 30 kHz)[1]. Additionally, the impact of the jet causes the water to splash and a number of droplets to also entrain bubbles. Towards the end of a breaking wave's life cycle the cavity of air trapped between the wave face and the plunging jet will collapse. This forms a large number of bubbles the majority of which are between 2.0 and 10.0 mm in radius (0.4 to 2 kHz)[78]. Given the high density of bubbles the remnants of the cavity act as a "bubble cloud." As discussed, earlier bubbles in a cloud tend to act as coupled oscillators with normal modes of oscillation much lower than that of individual bubbles[78,82]. The cavity collapse phase is thus responsible for frequencies between 0.1 and 0.5 kHz due to the bubble cloud, and higher frequencies up to ~2 kHz from individual oscillations[78,82]. It is also at this time that the plunging jet forms a shear zone along the wave surface which encircles the cavity remnants. Some bubbles will be pulled through this shear zone which can cause a bubble to fragment into two or more smaller fragments, which once again oscillate though at a higher frequency than their parent bubble[1,78,83]. For example, a large bubble oscillating at 3.1 kHz may produce two daughters one at 50 kHz and one at 32.3 kHz[78,84]. The intensity of the cavity collapse signature is far greater than that of the Jet period (or later shearing) thus when waves are continuously breaking in the marine environment it is the sound of these bubble clouds which dominates. Therefore, the acoustic signature of a breaking wave near the surface can most easily be recognised by low frequency signal between approximately 0.2-2 kHz[78,82] distinct from that of rain and gas seeps[36,57].

Deane & Stokes (2002) presented the average acoustic signature of (17) 10 cm tall plunging breakers, figure 9. Here one can clearly see the jet period, which is continuous throughout the breaking of the wave, responsible for the signal above 2 kHz with the majority of the sound generated below 10 kHz. The cavity collapse period can also be clearly identified as a quick (~0.3 s) low frequency burst centred around 0.3 kHz[78,84]. It should be intuitive that the acoustic signature (or rather the resulting bubble cloud) of a wave is a consequence of its size (and the style of breaking), which is typically a function of wind speed. Thus, by observing the breaking of a wave one could infer the acoustic signal or vice versa.

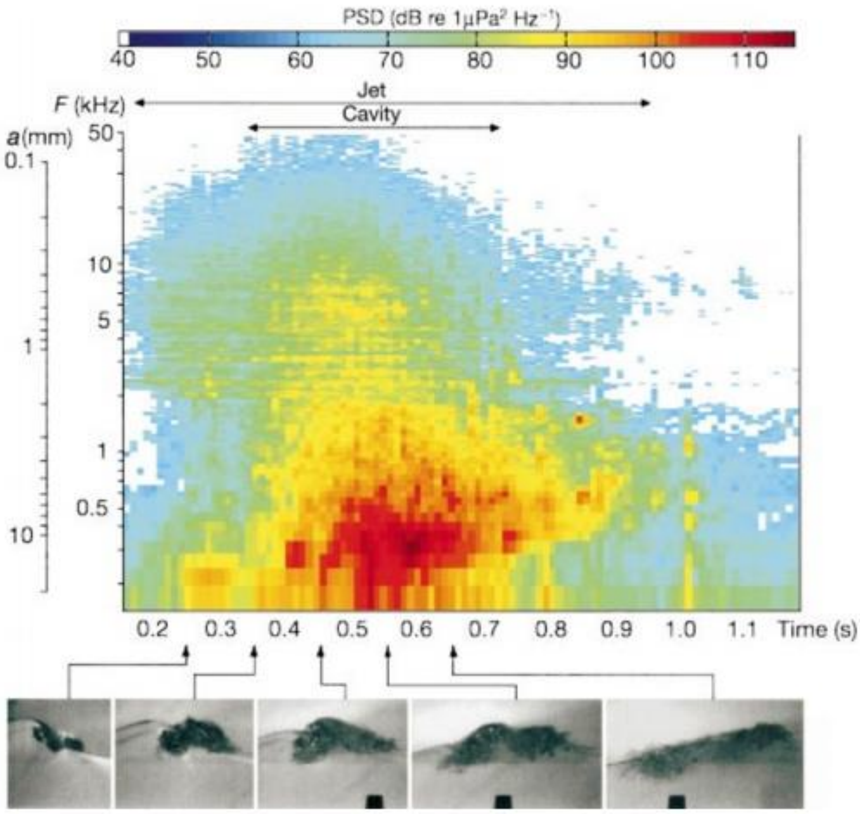

Figure 9; Spectrogram of wave noise calculated from an average of 17 breaking events. Note the “Jet” and “cavity” phases. The colour contours represent sound intensity plotted in a decibel scale (the intensity if referenced to 1 μPa^{2}Hz^{-1}) versus frequency and time. The log scale labelled “a” on the left-hand side indicates the radius of a bubble resonant at the corresponding frequency of the frequency scale (F). The wave noise was measured by a hydrophone mounted in the wave flume beneath the bubble plume. The images plotted below the spectrogram show the sequence of flow features at different times during the acoustic emissions. From Deane and Stokes (2002)

Given the energetic and variable nature of breaking waves it is difficult to predict exactly what happens to the resulting bubbles postproduction. The exception to this is during Langmuir circulation, which is the slow shallow counter rotational vortices aligned with wind direction that develop when wind blows steadily over a body of water, which have been extensively analysed. After formation Langmuir circulation, can carry wave generated bubbles up to 10 m below the surface[85]. In wind speeds >7 m/s this has been known to result in linear bubble clouds orientated parallel to wind direction[1]. These *Langmuir bubble clouds* consist of bubbles produced throughout the lifecycle of a wave (jet and cavity collapse phase) as well as potentially those entrained by rainfall. Individual bubbles in the cloud will naturally shrink due to dissolution and eventually disappear[86], however a high concentration of bubbles may delay this process and a continued supply of freshly generated bubbles can allow the cloud as a whole to persist as long as circulation is active.[1,86,87] The clouds generally have void fractions between 10^{-4} and 10^{-5}% that is assumed to be uniform in the horizontal plane but falls off exponentially with depth[1,81,88,89].

As the speed of sound depends on the inertia and stiffness of the material it is passing through the speed of sound in a bubble cloud (or "bubbly liquid") differs from that of pure water. As gas is less dense than water, sound waves travel more slowly through bubble clouds, becoming slower the larger and more numerous the bubbles are, i.e., the larger the void fraction[90,91]. If there is a distribution of bubble sizes within a cloud, such that $n_n^{gr}(z,R)dR_0$ is the number of bubbles per unit volume at depth z having a radii between R_0 and $R_0 + dR_0$, the speed of sound in a cloud c_c is given by[87];

$$c_c(z,\omega) = c\left\{1 - (2\pi c^2)\int_{R_0=0}^{\infty}\frac{R_0}{\omega^2}\left(\frac{(\omega_0/\omega)^2 - 1}{\{(\omega_0/\omega)^2 - 1\}^2 + d^2}\right)n_n^{gr}(z,R)dR_0\right\}, \tag{14}$$

where d is the dimensionless damping constant for a single bubble, and ω_0 being the resonant circular frequency of the bubble given by $\omega_0 = 2\pi f_0$.

Given the above, and the fact surface generated bubble clouds tend to decrease in concentration with depth, one can see how the presence of breaking waves can result in an ocean model where sound speed increases noticeably with depth within the upper ~10 m[1,92–96]. In such a scenario downward propagating sound waves will tend to turn, due to refraction, bending upwards back towards the surface. Similarly, upward propagating waves will also turn, refracting downwards. Repeating this cycle can result in the horizontal propagation of sound waves, trapping acoustic energy in the near surface[83,89]. In terms of wave acoustics, Farmer and Vagle (1989) and Buckingham (1991) both suggested that for a given mode the signal becomes evanescent (unable to propagate further) below certain "extinction" depth. They suggest trapping of sound in such a waveguide might influence the ambient acoustic spectra of wave noise and that by observing certain "drop out frequencies" one could infer the bubble size population generated by breaking waves, though Buckingham argues the loss of signal alone is not sufficient for a full analysis[94,95]. Unfortunately, the latter appears to be correct as despite numerous attempts in the following years little progress has been made inverting bubble populations from wave acoustics[90,91].

Accounting for the bubble cloud effects Deane & Stokes (2010) presented a model for calculating the underwater noise of a single breaking wave at a distance r with good agreement with experimental observations. Here, assuming wave noise is superposition of oscillations from generated bubbles, the creation times of bubbles being uniform and randomly distributed throughout the breaking period, the Power spectrum is given by

$$P(\omega, r) = \int_V \int_{a_{min}}^{a_{max}} \lambda(a, r) |\gamma(\omega, a) \alpha(\omega, a)|^2 \, da dV, \tag{15}$$

where a_{min} and a_{max} are the minimum and maximum bubble sizes generated, V is the plume volume, $\lambda(a, r)$ is the rate at which bubbles are generated, $\gamma(\omega, a)$ and $\alpha(\omega, a)$ are the Fourier transforms of the convolution of free-space bubble pulses and Greens function for the medium of propagation respectively[83].

With an understanding of the individual acoustic signal of a breaking wave and the manner in which bubble clouds effect the near surface, one might assume calculating the resulting signal of multiple breaking waves would be straightforward. After all, an observer, at a given depth, will record a signal that is the superposition of all the waves breaking above it at any given moment. Given a large enough area and a large enough number of waves, i.e., an ocean, one can assume a constant number of waves are breaking resulting in a constant "ambient" noise, as was the case with rainfall. Indeed, if all the waves were identical and occurring in some symmetrical pattern around the recorder, we could attempt to estimate the signal via theoretical calculations. However, this is not realistic and would be of little practical use, a range of breaking wave size and styles will always exist distributed erratically along the sea surface[79,80,92,93]. Additionally, a detailed understanding of the size distribution of bubbles generated in a breaking wave $\lambda(a, r)$ in equation 15 is required, something lacking outside of easily replicable waves[83].

For simplicity's sake the seminal work of Knudsen et al., (1948) and Wenz (1962) describing the ambient sound pressure level (SPL) in the ocean at different wind speeds using field observations, seen in figure 6, is still relevant[9,88,96]. Starting at around 0.20 kHz rising 3-5 dB re 1μPa^2/Hz to a peak at approximately 0.5 kHz (consistent with the above discussion) before dropping off slowly, ~25 dB re 1μPa^2/Hz by 10 kHz, with peak sound pressure levels of 60 and 73 dB re 1μPa^2/Hz respectively for wind speeds of 3.4- 5.5 m/s and 17.2- 20.7 m/s[81,88,96,97]. This does not generally cover strong gales (wind speed > 20.8 m/s), as during higher wind speeds it becomes difficult to identify periods of pure wind noise (i.e., non-rain contaminated).

Despite the complexity of the task however, many still wish to be able to calculate the ambient noise of breaking waves e.g., for storm monitoring[60,61,65,96,98] or studying ocean atmospheric mixing[78,99]. The most widespread approach it via WOTAN (Wind Observations Through Ambient Noise) calculations. Here observations of the ambient noise from breaking waves has been correlated with wind speed through numerous studies to empirically map their relationship[88,96]. Originally this work was done with the intent of estimating wind speed based on ambient wave noise, but the reverse should also possible (calculating ambient wave noise based on wind speed).

Using past studies and their own data Vagle et al., (1990) determined that the source sound level at a depth of 1 m from breaking waves was given by

$$SSL_0 = q \log f + G, \tag{16}$$

where q is the slope of the logarithmic spectrum of the wind generated sound which they find to be equal to -19.0 dB/decade (in good agreement with past estimates[81]). G is a variable function of wind speed. Vagle et al., (1990) determined values for G between set wind speeds which we note approximately follows $G = 1.3U_{10}$+56 (U_{10} being the wind speed 10 m above water level). Unfortunately, this sound level equation only holds true for low wind speeds ($U_{10} \leq$ 15 m/s) and below a certain critical frequency, $\log f_c = 1.9 - 0.07U_{10}$[99].

Zhao et al. (2014) expanded upon this work and by studying the underwater acoustics of typhoons using Lagrangian floats. Figure 10 displays the spectral content they observed at a range of high wind speeds from a number of floats. They noted that low frequency sound (<1 kHz) monotonically increased with wind speed while intermediate and higher frequencies initially increase then decrease with wind speed. They presented the following empirical equation to calculate the sound pressure level of a given frequency in wind speeds up to 50 m/s[96].

$$SPL = S_{noise} + S_{10} \frac{\left(U_{10}/_{10}\right)^{n_{lf}}}{1 + \left(U_{10}/_{f_{peak}}\right)^{n_{hf}}},$$

(17)

where S_{noise} is the noise floor, S_{10} is the sound level at 10 ms^{-1} wind, f_{peak} controls the wind speed with the sound level maximum and n_{lf} / n_{hf} are values which control the increasing / decreasing in lower/higher wind conditions. All of these values are a function of the target frequency though the exact relationship is not fully understood nor linear, determined instead via least square fitting of observations[96]. Consequently, real time analysis of wind speed via acoustics is still an emerging field. While highly promising this approach needs to be tested in multiple environments many more times, especially if the underlying variables are to be better understood[61,88,96,100–103].

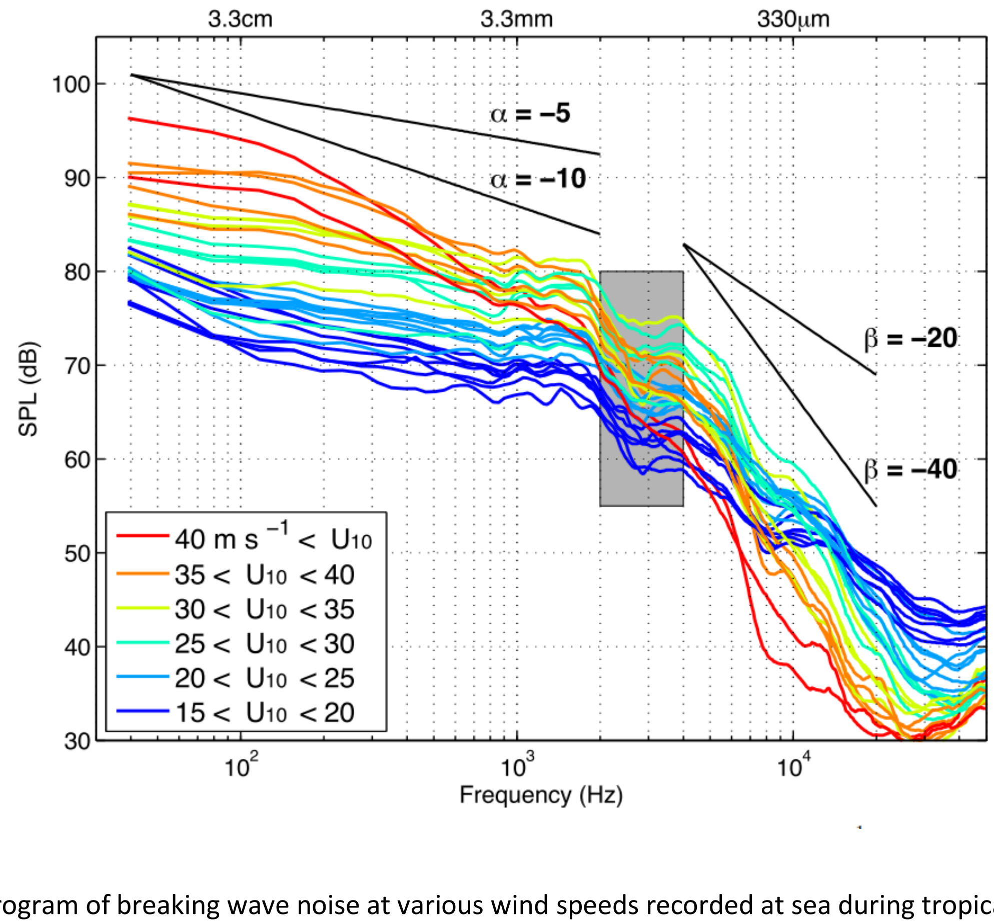

Figure 10; spectrogram of breaking wave noise at various wind speeds recorded at sea during tropical cyclones. Each curve averages all spectra in 5 ms^{-1} wind speed bins from measurements at depth > 2m of a single float, multiple curves of the same colour denote observations from multiple floats. The four black lines show representative spectral slopes at low (α) and high (β) frequencies. Gray box shows the transition frequency (2-4 kHz) between the two slope regions. The dip in sound level near 3 kHz may be an instrumental effect. Taken from Zhao et al. (2014)

It should be apparent from the above that accurately predicting the acoustic signal recorded at a hydrophone as a result of breaking waves, at any given wind speed, is an exceedingly difficult task especially at gale force winds (>17.6 m/s)[88,96], and particularly without some prior observations for calibration. Furthermore, many empirical WOTAN studies themselves are intrinsically flawed for the purpose of calculating noise levels at depth as they only study the effects of wind on specific frequencies. Additionally, without a better understanding of the affect bubble clouds have on the downward propagating of the signal estimations at depth (>100 m) are highly speculative.

In summary the acoustic signature of a breaking wave is primarily the result of bubble cloud generation during the final cavity collapse phase of a wave's life cycle. While individual bubble frequencies range from 0.4 to 2.0 kHz the frequency of the bubble cloud itself is typically lower, at 0.1 to 0.5 kHz. The exact frequency spectrum depends on the properties of the wave itself, which is usually a consequence of wind speed, so can be highly variable even under laboratory conditions. Bubbles generated by breaking waves can be pulled down up to 10m by Langmuir currents where they can create steep sound speed profiles with depth, possibly trapping select acoustic signals. The highly dynamic and unpredictable nature of breaking waves make predicting ambient noise from multiple breaking waves difficult, especially in gale force winds. "Wind Observations Through Ambient Noise" allow for measurements of wind speed via the ambient noise of wave action based on empirical observations but are insufficient for calculating ambient noise at depth. Knudsen curves are still the most commonly used prediction of ambient noise from wave action, with a positively skewed peak at around 0.5 kHz increasing in intensity with wind speed.

Conclusion

Bubbles have subtle, yet far reaching effects on marine acoustics. The initial formation of a bubble triggers simple harmonic motion at a natural frequency, known as the Minnaert frequency, which is approximately inversely proportional to its radius. Thus, by observing the acoustic signature of a bubble one can determine its size. While the sound of a single bubble is low energy, the continuous release of multiple bubbles can have a significant impact on the ambient marine soundscape. In order to accurately predict the ambient noise produced by either a gas seep, rainfall, or breaking waves one must have a detailed understanding of the size distribution of bubbles being generated. Unfortunately, it is all but impossible to predict the size of bubbles released. However, it is possible to use observations of ambient noise to infer the characteristics of these sources; the flux from a gas seep, the intensity of rainfall and the wind speed resulting in breaking waves.

Further Reading

The following sources are recommended for continuing research in each of the areas introduced in this chapter.

Bubble Physics

- Leighton, T. G. The Freely-oscillating Bubble. in *The Acoustic Bubble* 129–286 (Elsevier, 1994). doi:10.1016/B978-0-12-441920-9.50008-0.

Subsea Gas Seep Acoustics

- Leighton, T. G. & White, P. R. Quantification of undersea gas leaks from carbon capture and storage facilities, from pipelines and from methane seeps, by their acoustic emissions. *Proceedings of the Royal Society A: Mathematical, Physical and Engineering Sciences* **468**, 485–510 (2012).
- Bergès, B. J. P., Leighton, T. G. & White, P. R. Passive acoustic quantification of gas fluxes during controlled gas release experiments. *International Journal of Greenhouse Gas Control* **38**, 64–79 (2015).

Rainfall Acoustics

- Serra, Y. L. Precipitation measurements from the Tropical Moored Array: A review and look ahead. *Quarterly Journal of the Royal Meteorological Society* **144**, 221–234 (2018).
- Ma, B. B. & Nystuen, J. A. Passive Acoustic Detection and Measurement of Rainfall at Sea. *Journal of Atmospheric and Oceanic Technology* **22**, 1225–1248 (2005).
- Pumphrey, H. C. & Crum, L. A. Free oscillations of near-surface bubbles as a source of the underwater noise of rain. *The Journal of the Acoustical Society of America* **87**, 142–148 (1990).
- Pumphrey, H. C. & Elmore, P. A. The entrainment of bubbles by drop impacts. *Journal of Fluid Mechanics* **220**, 539–567 (1990).
- Pumphrey, H.C., Walton, A.J., 1988. Experimental study of the sound emitted by water drops impacting on a water surface. Eur. J. Phys. 9, 225–231. https://doi.org/10.1088/0143-0807/9/3/011

Breaking Wave Acoustic

- Deane, G. B. & Stokes, M. D. Scale dependence of bubble creation mechanisms in breaking waves. *Nature* **418**, 839–844 (2002).
- Deane, G. B. & Stokes, M. D. Model calculations of the underwater noise of breaking waves and comparison with experiment. *The Journal of the Acoustical Society of America* **127**, 3394–3410 (2010).
- Zhao, Z., D'Asaro, E. A. & Nystuen, J. A. The Sound of Tropical Cyclones. *Journal of Physical Oceanography* **44**, 2763–2778 (2014).
- Leighton, T. G. The Freely-oscillating Bubble. in *The Acoustic Bubble* 129–286 (Elsevier, 1994). doi:10.1016/B978-0-12-441920-9.50008-0
- Vagle, S., Large, W. G. & Farmer, D. M. An Evaluation of the WOTAN Technique of Inferring Oceanic Winds from Underwater Ambient Sound. *Journal of Atmospheric and Oceanic Technology* **7**, 576–595 (1990).

Appendix

Minnaert Frequency Derivation

The following is a derivation of the Minnaert equation following Leighton (1994).

We can find the Kinetic Energy, ϕ_K, of the water surrounding a bubble by integrating over shells of liquid from the bubble wall to infinity. A shell of radius r and a thickness dr has a mass of $4\pi r^2 \rho dr$ (ρ being the density of water), thus the kinetic energy of the surrounding water is.

$$\varphi_K = \int_R^{\infty} (4\pi r^2 \rho \, dr)\dot{r}^2 \tag{A1}$$

The mass of liquid flowing in time dt through any spherical surface around the bubble is $4\pi r^2 \dot{r} \rho dt$. Assuming the liquid is incompressible then by conservation of mass this general flow can be equated to the flow at the bubble surface which can be shown to be $\dot{r}/\dot{R} = R^2/r^2$. Substituting this into the above gives.

$$\varphi_K = 2\pi R^3 \rho \dot{R}^2 \tag{A2}$$

Kinetic Energy is a maximum at the equilibrium position (as with any harmonic oscillator) when $R = R_0$ and $\dot{R} = i\omega_0 R_{\varepsilon 0} e^{i\omega_0 t}$ implying that $|\dot{R}|^2 = (\omega_0 R_{\varepsilon 0})^2$. Thus, the maximum value of the kinetic energy is

$$\varphi_{KMax} = \frac{1}{2} m_{RF}^{rad} (\omega_0 R_{\varepsilon 0})^2 = 2\pi {R_0}^3 \rho (\omega_0 R_{\varepsilon 0})^2 \tag{A3}$$

where m_{RF}^{rad} is the radiation mass of the bubble in radius-force frame. This mass is the effective inertia of the liquid component of the oscillating system which the pulsating bubble represents i.e., $m_{RF}^{rad} = 4\pi {R_0}^3 \rho$. It arises from the liquid that is transmitting acoustic waves and is the only inertia considered by the Minnaert derivation.

Through conservation of energy, maximum kinetic energy φ_{KMax} must equal maximum internal energy φ_{PMax} which occurs when $R = R_0 \pm R_{\varepsilon 0}$ and $\dot{R} = 0$. The work done compressing the bubble from equilibrium volume V_0 (at radius R_0) to minimum volume V_{min} (at radius $R_0 - R_{\varepsilon 0}$) is the integral of $-(p_g - p_0)dV$ where p_g is the gas pressure and p_0 is the hydrostatic liquid pressure outside the bubble.

$$\varphi_{PMax} = -\int_{V_{max}}^{V_{min}} (p_g - p_0)\, dV = -\int_{R_0}^{R_0 - R_{\varepsilon 0}} (p_g - p_0) 4\pi r^2\, dr$$

(A4)

Minnaert derived his equation assuming that the gas behaved adiabatically, i.e. that there was no heat flow across the bubble wall. This was adapted by the introduction of the polytropic index κ (which takes a value equal to unity when the gas behaves isothermally and equals the ratio of the specific heat of the gas at constant pressure to that at constant volume, when the gas behaves adiabatically)[8]. Assuming the gas behaves polytropically so that $p_g V^\kappa = constant$ then since $R_\varepsilon = R - R_0$ by equating the pressure and volume condition at equilibrium to those when the bubble attains minimum volume gives.

$$p_g (R_0 + R_\varepsilon)^{3k} = p_0 {R_0}^{3k}$$

(A5)

for small displacements, the binomial expansion of this is.

$$p_0 - p_g \approx \frac{3\kappa R_\varepsilon p_0}{R_0}$$

(A5)

substituting this into the maximum internal energy φ_{PMax} with the use to first order $R_\varepsilon = R - R_0$ coordinates gives.

$$\varphi_{PMax} = \int_0^{R_{\varepsilon 0}} \frac{3\kappa R_\varepsilon p_0}{R_0} 4\pi {R_0}^2\, dR_\varepsilon = 6\pi\kappa p_0 R_0 {R_{\varepsilon 0}}^2$$

(A6)

this allows us to equate the maximum kinetic energy and maximum potential energy

$$\varphi_{KMax} = 2\pi {R_0}^3 \rho(\omega_0 R_{\varepsilon 0})^2 = 6\pi\kappa p_0 R_0 {R_{\varepsilon 0}}^2 = \varphi_{PMax}$$

(A7)

which can be solved for the resonance circular frequency ω_0;

$$\omega_0 = \frac{1}{R_0}\sqrt{\frac{3\kappa p_0}{\rho}}$$

(A8)

and finally using $\omega_0 = 2\pi f_M$ gives us the Minnaert frequency equation.

$$f_M = \frac{1}{2\pi R_0}\sqrt{\frac{3\kappa p_0}{\rho}}$$

(A9)

Symbology

SYMBOL	DEFINTION
a_{min}	Minimum bubble size generated
a_{max}	Maximum bubble size generated
$B(R_0)$	Bubble size distribution
c	Speed of sound in water
c_c	Speed of sound through a bubble cloud
d	Dimensionless damping constant for a single bubble $= 2\beta/\omega$
D	initial dipole strength of the bubble
f	Frequency
f_{peak}	Peak frequency
f_M	Minnaert frequency – oscillation frequency of a bubble as predicted by Minnaert equation
f_0	Natural frequency of a bubble oscillation
G	A variable function of wind speed
h	Distance from the *centre* of the bubble to the surface of the water
I_{Rain}	Intensity of rainfall beneath the surface at a given frequency
ISL_{Rain}	Intensity spectrum level of rainfall beneath the surface at a given frequency
l	loaded length of spring
l_0	unloaded length of spring
L_d	Diameter of water droplet
m_{RF}^{rad}	Radiation mass of bubble in radius force frame
n	Mode number
$n(f)$	Number of bubbles entrained per second by rainfall
n_{lf}	A quantity controlling the increasing slope of wave noise in lower wind conditions
n_{hf}	A quantity controlling the decreasing slope of wave noise in higher wind conditions
$n_n^{gr}(z,R)dR_0$	Number of bubbles per unit volume at depth z having a radii between R_0 and $R_0 + dR_0$
N_b	Number of identical bubbles in a bubble cloud
p_g	Gas pressure inside bubble
p_0	Hydrostatic liquid pressure outside the bubble
p_v	Vapour pressure
$P(\omega,r)$	Power spectrum of a breaking wave
q	Quality factor
Q_w	Slope of the logarithmic spectrum of the wind generated sound
r	Radial distance
R	Radius of Bubble wall
R_0	Equilibrium radius of bubble
R_ε	Displacement of the bubble wall from equilibrium radius
$R_{\varepsilon 0}$	Maximum displacement of bubble wall from equilibrium radius
$R_{\epsilon 0i}$	Initial amplitude of displacement of the bubble wall
R_{max}	Maximum radius of bubble
R_{min}	Minimum radius of bubble
S	Column vector containing the measured spectrum $S(\omega_k)$
$S(\omega)$	Power spectral density of a marine gas seep
S_{10}	Sound level at 10 ms^{-1} wind
S_{noise}	Noise floor
S_{rain}	Rainfall rate
SPL	Sound pressure level
SPL_{5kHZ}	Sound pressure level at 5 kHz
SSL_0	Source sound level of breaking waves at a depth of 1m
t	Time
u	Impact mach number
u_d	Impact speed of water droplet

$\boldsymbol{U_{10}}$	Wind speed 10 m above water level
$\boldsymbol{V}$	Volume of bubble plume
$\boldsymbol{V_0}$	Equilibrium bubble volume
$\boldsymbol{V_{min}}$	Minimum bubble volume
$\boldsymbol{VF}$	Void Fraction
$\boldsymbol{z}$	Depth below sea surface
$\boldsymbol{\alpha(\omega, a)}$	Fourier transform of the Greens function for the medium of propagation respectively
$\boldsymbol{\gamma(\omega, a)}$	Fourier transform of the convolution of free-space bubble pulses
$\boldsymbol{\delta_{tot}}$	Total damping constant for bubble pulsation at resonance
$\boldsymbol{\varepsilon}$	Displacement from equilibrium
$\boldsymbol{\theta}$	Polar angle, angle between observer and source relative to the z axis
$\boldsymbol{\varphi_K}$	Kinetic energy
$\boldsymbol{\varphi_{KMax}}$	Maximum kinetic energy
$\boldsymbol{\varphi_{PMax}}$	Maximum internal energy
$\boldsymbol{\kappa}$	Polytropic index
$\boldsymbol{\sigma}$	Surface tension
$\boldsymbol{\eta}$	Shear viscosity
$\boldsymbol{\rho}$	Density of water
$\boldsymbol{\omega}$	Angular frequency $= 2\pi f$
$\boldsymbol{\omega_0}$	Angular resonate frequency
$\boldsymbol{\Psi(n)}$	Bubble generation rate (for marine gas seep)

Bibliography

1. Leighton, T. G. The Freely-oscillating Bubble. in *The Acoustic Bubble* 129–286 (Elsevier, 1994). doi:10.1016/B978-0-12-441920-9.50008-0.

2. Longuet-Higgins, M. S., Kerman, B. R. & Lunde, K. The release of air bubbles from an underwater nozzle. *Journal of Fluid Mechanics* **230**, 365–390 (1991).

3. Czerski, H. & Deane, G. B. Contributions to the acoustic excitation of bubbles released from a nozzle. *The Journal of the Acoustical Society of America* **128**, 2625–2634 (2010).

4. Phelps, A. D., Ramble, D. G. & Leighton, T. G. The use of a combination frequency technique to measure the surf zone bubble population. *The Journal of the Acoustical Society of America* **101**, 1981–1989 (1997).

5. Minnaert, M. XVI. On musical air-bubbles and the sounds of running water. *The London, Edinburgh, and Dublin Philosophical Magazine and Journal of Science* **16**, 235–248 (1933).

6. Ainslie, M. A. & Leighton, T. G. Review of scattering and extinction cross-sections, damping factors, and resonance frequencies of a spherical gas bubble. *The Journal of the Acoustical Society of America* **130**, 3184–3208 (2011).

7. Walton, A. J., Gunn, M. G. & Reynolds, G. T. The Quality Factor of Oscillating Bubbles as an Indication of Gas Content with Particular Reference to Methane. *IEEE Journal of Oceanic Engineering* **30**, 924–926 (2005).

8. Leighton, T. G. & Walton, A. J. An experimental study of the sound emitted from gas bubbles in a liquid. *European Journal of Physics* **8**, 98–104 (1987).

9. Medwin, H. & Beaky, M. M. Bubble sources of the Knudsen sea noise spectra. *The Journal of the Acoustical Society of America* **86**, 1124–1130 (1989).

10. Pumphrey, H. C. & Crum, L. A. Free oscillations of near-surface bubbles as a source of the underwater noise of rain. *The Journal of the Acoustical Society of America* **87**, 142–148 (1990).

11. Leighton, T. G., White, P. R. & Schneider, M. F. The detection and dimension of bubble entrainment and comminution. *The Journal of the Acoustical Society of America* **103**, 1825–1835 (1998).

12. Leighton, T. G. & White, P. R. Quantification of undersea gas leaks from carbon capture and storage facilities, from pipelines and from methane seeps, by their acoustic emissions. *Proceedings of the Royal Society A: Mathematical, Physical and Engineering Sciences* **468**, 485–510 (2012).

13. Leighton, T. G. The frequency analysis of transients. *European Journal of Physics* **9**, 69–70 (1988).

14. LEIGHTON, T. G. From seas to surgeries, from babbling brooks to baby scans: the acoustics of gas bubbles in liquids. *International Journal of Modern Physics B* **18**, 3267–3314 (2004).

15. Strasberg, M. The Pulsation Frequency of Nonspherical Gas Bubbles in Liquids. *The Journal of the Acoustical Society of America* **25**, 536–537 (1953).

16. Lu, N. Q., Prosperetti, A. & Yoon, S. W. Underwater noise emissions from bubble clouds. *IEEE Journal of Oceanic Engineering* **15**, 275–281 (1990).

17. Judd, A. G. The global importance and context of methane escape from the seabed. *Geo-Marine Letters* **23**, 147–154 (2003).

18. Knittel, K. & Boetius, A. Anaerobic Oxidation of Methane: Progress with an Unknown Process. *Annual Review of Microbiology* **63**, 311–334 (2009).

19. McGinnis, D. F., Greinert, J., Artemov, Y., Beaubien, S. E. & Wüest, A. Fate of rising methane bubbles in stratified waters: How much methane reaches the atmosphere? *Journal of Geophysical Research* **111**, C09007 (2006).

20. Roche, B., Bull, J.M., Marin-Moreno, H., Leighton, T.G., Suarez, I.F., Tholen, M., White, P.R., Provenzano, G., Lichtschlag, A., Li, J., F, Faggetter Time-lapse imaging of CO2 migration within near-surface sediment during a controlled sub-seabed release experiment. *International Journal of Greenhouse Gas Control (IN REVIEW)* (2020).

21. Johnson, B. D., Barry, M. A., Boudreau, B. P., Jumars, P. A. & Dorgan, K. M. In situ tensile fracture toughness of surficial cohesive marine sediments. *Geo-Marine Letters* **32**, 39–48 (2012).

22. Johnson, B. D., Boudreau, B. P., Gardiner, B. S., and Maass, R. Mechanical response of sediments to bubble growth. *Marine Geology* **187**, 247–363 (2002).

23. Jain, A. K. & Juanes, R. Preferential Mode of gas invasion in sediments: Grain-scale mechanistic model of coupled multiphase fluid flow and sediment mechanics. *Journal of Geophysical Research* **114**, B08101 (2009).

24. Maksimov, A. O., Burov, B. A., Salomatin, A. S. & Chernykh, D. v. Sounds of Undersea Gas Leaks. in *Underwater Acoustics and Ocean Dynamics* 107–116 (Springer Singapore, 2016). doi:10.1007/978-981-10-2422-1_15.

25. Algar, C. K., Boudreau, B. P. & Barry, M. A. Initial rise of bubbles in cohesive sediments by a process of viscoelastic fracture. *Journal of Geophysical Research* **116**, B04207 (2011).

26. Boudreau, B. P. *et al.* Bubble growth and rise in soft sediments. *Geology* **33**, 517 (2005).

27. Boudreau, B. P. The physics of bubbles in surficial, soft, cohesive sediments. *Marine and Petroleum Geology* **38**, 1–18 (2012).

28. Vazquez, A., Manasseh, R. & Chicharro, R. Can acoustic emissions be used to size bubbles seeping from a sediment bed? *Chemical Engineering Science* **131**, 187–196 (2015).

29. Suess, E. Marine cold seeps and their manifestations: geological control, biogeochemical criteria and environmental conditions. *International Journal of Earth Sciences* **103**, 1889–1916 (2014).

30. Coughlan, M. *et al.* Geological settings and controls of fluid migration and associated seafloor seepage features in the north Irish Sea. *Marine and Petroleum Geology* **123**, 104762 (2021).

31. Hovland, M. On the self-sealing nature of marine seeps. *Continental Shelf Research* **22**, 2387–2394 (2002).

32. Li, J. *et al.* Broadband acoustic inversion for gas flux quantification - application to a methane plume at Scanner Pockmark, central North Sea. *Journal of Geophysical Research: Oceans* (2020) doi:10.1029/2020JC016360.

33. Böttner, C. *et al.* Pockmarks in the Witch Ground Basin, Central North Sea. *Geochemistry, Geophysics, Geosystems* **20**, 1698–1719 (2019).

34. Leighton, T. G., K.J., F. & Field J.E. Acoustic and photographic studies of injected bubbles. *European Journal of Physics* **12**, 77--85 (1991).

35. Römer, M., Riedel, M., Scherwath, M., Heesemann, M. & Spence, G. D. Tidally controlled gas bubble emissions: A comprehensive study using long-term monitoring data from the NEPTUNE cabled observatory offshore Vancouver Island. *Geochemistry, Geophysics, Geosystems* **17**, 3797–3814 (2016).

36. Bergès, B. J. P., Leighton, T. G. & White, P. R. Passive acoustic quantification of gas fluxes during controlled gas release experiments. *International Journal of Greenhouse Gas Control* **38**, 64–79 (2015).

37. Sultan, N., Plaza-Faverola, A., Vadakkepuliyambatta, S., Buenz, S. & Knies, J. Impact of tides and sea-level on deep-sea Arctic methane emissions. *Nature Communications* **11**, 5087 (2020).

38. Boles, J. R., Clark, J. F., Leifer, I. & Washburn, L. Temporal variation in natural methane seep rate due to tides, Coal Oil Point area, California. *Journal of Geophysical Research: Oceans* **106**, 27077–27086 (2001).

39. Scandella, B. P. *et al.* Ephemerality of discrete methane vents in lake sediments. *Geophysical Research Letters* **43**, 4374–4381 (2016).

40. Klaucke, I., Weinrebe, W., Petersen, C. J. & Bowden, D. Temporal variability of gas seeps offshore New Zealand: Multi-frequency geoacoustic imaging of the Wairarapa area, Hikurangi margin. *Marine Geology* **272**, 49–58 (2010).

41. Riedel, M. *et al.* Distributed natural gas venting offshore along the Cascadia margin. *Nature Communications* **9**, 3264 (2018).

42. Leifer, I. Seabed bubble flux estimation by calibrated video survey for a large blowout seep in the North Sea. *Marine and Petroleum Geology* **68**, 743–752 (2015).

43. Wiggins, S. M., Leifer, I., Linke, P. & Hildebrand, J. A. Long-term acoustic monitoring at North Sea well site 22/4b. *Marine and Petroleum Geology* **68**, 776–788 (2015).

44. Leifer, I. & Patro, R. K. The bubble mechanism for methane transport from the shallow sea bed to the surface: A review and sensitivity study. *Continental Shelf Research* **22**, 2409–2428 (2002).

45. Muyakshin, S. I. & Sauter, E. The hydroacoustic method for the quantification of the gas flux from a submersed bubble plume. *Oceanology* **50**, 995–1001 (2010).

46. Ostrovsky, I., McGinnis, D. F., Lapidus, L. & Eckert, W. Quantifying gas ebullition with echosounder: the role of methane transport by bubbles in a medium-sized lake. *Limnology and Oceanography: Methods* **6**, 105–118 (2008).

47. Li, J. *et al.* Broadband Acoustic Inversion for Gas Flux Quantification—Application to a Methane Plume at Scanner Pockmark, Central North Sea. *Journal of Geophysical Research: Oceans* **125**, (2020).

48. Esposito, A., Giordano, G. & Anzidei, M. The 2002–2003 submarine gas eruption at Panarea volcano (Aeolian Islands, Italy): Volcanology of the seafloor and implications for the hazard scenario. *Marine Geology* **227**, 119–134 (2006).

49. Li, J. *et al.* Passive acoustic monitoring of a natural CO2 seep site – Implications for carbon capture and storage. *International Journal of Greenhouse Gas Control* **93**, 102899 (2020).

50. Li, J. *et al.* Acoustic and optical determination of bubble size disruptions - quantification of undersea gas emissions. *International Journal of Greenhouse Gas Control* (2020).

51. Greene, C. A. & Wilson, P. S. Laboratory investigation of a passive acoustic method for measurement of underwater gas seep ebullition. *The Journal of the Acoustical Society of America* **131**, EL61–EL66 (2012).

52. Roche, B. *et al.* Validating passive acoustic methods for gas flux quantification, offshore Panarea, Mediterranean Sea. *The Journal of the Acoustical Society of America* **146**, 2965–2965 (2019).

53. Chen, L., Trinh, V., Yang, W. & Mohanangam, K. Prediction of Bubble Generation Based on Acoustic Emission. *Acoustics Australia* **44**, 325–331 (2016).

54. Pumphrey, H. C. & Elmore, P. A. The entrainment of bubbles by drop impacts. *Journal of Fluid Mechanics* **220**, 539–567 (1990).

55. Pumphrey, H. C. & Walton, A. J. Experimental study of the sound emitted by water drops impacting on a water surface. *European Journal of Physics* **9**, 225–231 (1988).

56. Nystuen, J. A. Listening to Raindrops from Underwater: An Acoustic Disdrometer. *Journal of Atmospheric and Oceanic Technology* **18**, 1640–1657 (2001).

57. Ma, B. B. & Nystuen, J. A. Passive Acoustic Detection and Measurement of Rainfall at Sea. *Journal of Atmospheric and Oceanic Technology* **22**, 1225–1248 (2005).

58. Black, P. G., Proni, J. R., Wilkerson, J. C. & Samsury, C. E. Oceanic Rainfall Detection and Classification in Tropical and Subtropical Mesoscale Convective Systems Using Underwater Acoustic Methods. *Monthly Weather Review* **125**, 2014–2042 (1997).

59. Serra, Y. L. Precipitation measurements from the Tropical Moored Array: A review and look ahead. *Quarterly Journal of the Royal Meteorological Society* **144**, 221–234 (2018).

60. Yang, J., Riser, S., Nystuen, J., Asher, W. & Jessup, A. Regional Rainfall Measurements Using the Passive Aquatic Listener During the SPURS Field Campaign. *Oceanography* **28**, 124–133 (2015).

61. Pensieri, S. *et al.* Underwater Acoustic Measurements to Estimate Wind and Rainfall in the Mediterranean Sea. *Advances in Meteorology* **2015**, 1–18 (2015).

62. Taylor, W. O., Anagnostou, M. N., Cerrai, D. & Anagnostou, E. N. Machine Learning Methods to Approximate Rainfall and Wind From Acoustic Underwater Measurements (February 2020). *IEEE Transactions on Geoscience and Remote Sensing* 1–12 (2020) doi:10.1109/TGRS.2020.3007557.

63. Nystuen, J. A., Anagnostou, M. N., Anagnostou, E. N. & Papadopoulos, A. Monitoring Greek Seas Using Passive Underwater Acoustics. *Journal of Atmospheric and Oceanic Technology* **32**, 334–349 (2015).

64. Ashokan, M., Latha, G. & Ramesh, R. Analysis of shallow water ambient noise due to rain and derivation of rain parameters. *Applied Acoustics* **88**, 114–122 (2015).

65. Anagnostou, M. N., Nystuen, J. A., Anagnostou, E. N., Nikolopoulos, E. I. & Amitai, E. Evaluation of Underwater Rainfall Measurements During the Ionian Sea Rainfall Experiment. *IEEE Transactions on Geoscience and Remote Sensing* **46**, 2936–2946 (2008).

66. Nystuen, J. A., Amitai, E., Anagnostou, E. N. & Anagnostou, M. N. Spatial averaging of oceanic rainfall variability using underwater sound: Ionian sea rainfall experiment 2004. *The Journal of the Acoustical Society of America* **123**, 1952–1962 (2008).

67. Nystuen, J. A. Rainfall measurements using underwater ambient noise. *The Journal of the Acoustical Society of America* **79**, 972–982 (1986).

68. Scrimger, J. A., Evans, D. J., McBean, G. A., Farmer, D. M. & Kerman, B. R. Underwater noise due to rain, hail, and snow. *The Journal of the Acoustical Society of America* **81**, 79–86 (1987).

69. Pumphrey, H. C. Sources of ambient noise in the ocean an experimntal investigation. (1989).

70. Nystuen, J. A. & Selsor, H. D. Weather Classification Using Passive Acoustic Drifters. *Journal of Atmospheric and Oceanic Technology* **14**, 656–666 (1997).

71. Nystuen, J. A., McPhaden, M. J. & Freitag, H. P. Surface Measurements of Precipitation from an Ocean Mooring: The Underwater Acoustic Log from the South China Sea*. *Journal of Applied Meteorology* **39**, 2182–2197 (2000).

72. Medwin, H., Kurgan, A. & Nystuen, J. A. Impact and bubble sound from raindrops at normal and oblique incidence. *The Journal of the Acoustical Society of America* **88**, 413–418 (1990).

73. Ma, B. B. & Nystuen, J. A. Detection of Rainfall Events Using Underwater Passive Aquatic Sensors and Air–Sea Temperature Changes in the Tropical Pacific Ocean. *Monthly Weather Review* **135**, 3599–3612 (2007).

74. Cavaleri, L. & Bertotti, L. Rain on Generative Seas. *Geophysical Research Letters* **45**, 7049–7056 (2018).

75. Wu, J. Oceanic Whitecaps and Sea State. *Journal of Physical Oceanography* **9**, 1064–1068 (1979).

76. Cavaleri, L. Rain, Wave Breaking and Spray. in *Recent Advances in the Study of Oceanic Whitecaps* 65–75 (Springer International Publishing, 2020). doi:10.1007/978-3-030-36371-0_5.

77. Holthuijsen, L. H. *Waves in Oceanic and Coastal Waters*. (Cambridge University Press, 2007). doi:10.1017/CBO9780511618536.

78. Deane, G. B. & Stokes, M. D. Scale dependence of bubble creation mechanisms in breaking waves. *Nature* **418**, 839–844 (2002).

79. Bass, S. J. & Hay, A. E. Ambient noise in the natural surf zone: wave-breaking frequencies. *IEEE Journal of Oceanic Engineering* **22**, 411–424 (1997).

80. Manasseh, R. *et al.* Passive Acoustic Determination of Wave-Breaking Events and Their Severity across the Spectrum. *Journal of Atmospheric and Oceanic Technology* **23**, 599–618 (2006).

81. Farmer, D. M. & Vagle, S. On the determination of breaking surface wave distributions using ambient sound. *Journal of Geophysical Research* **93**, 3591 (1988).

82. Carey, W. M. & Bradley, M. P. Low-frequency ocean surface noise sources. *The Journal of the Acoustical Society of America* **78**, S1–S2 (1985).

83. Deane, G. B. & Stokes, M. D. Model calculations of the underwater noise of breaking waves and comparison with experiment. *The Journal of the Acoustical Society of America* **127**, 3394–3410 (2010).

84. Thorpe, S. A. On the Clouds of Bubbles Formed by Breaking Wind-Waves in Deep Water, and their Role in Air -- Sea Gas Transfer. *Philosophical Transactions of the Royal Society of London. Series A, Mathematical and Physical Sciences* **304**, 155–210 (1982).

85. Monahan, E. C. & Lu, M. Acoustically relevant bubble assemblages and their dependence on meteorological parameters. *IEEE Journal of Oceanic Engineering* **15**, 340–349 (1990).

86. Liang, J.-H., McWilliams, J. C., Sullivan, P. P. & Baschek, B. Modeling bubbles and dissolved gases in the ocean. *Journal of Geophysical Research* **116**, C03015 (2011).

87. Acoustical Oceanography: Principles and Applications. By C. S. Clay and H. Medwin New York: John Wiley & Sons, 1977. xviii, 544 pp. (Ocean Engineering: A Wiley Series.) Price £20·65/$34·95. *Journal of the Marine Biological Association of the United Kingdom* **58**, 543–543 (1978).

88. Vagle, S., Large, W. G. & Farmer, D. M. An Evaluation of the WOTAN Technique of Inferring Oceanic Winds from Underwater Ambient Sound. *Journal of Atmospheric and Oceanic Technology* **7**, 576–595 (1990).

89. Farmer, D. M., Deane, G. B. & Vagle, S. The influence of bubble clouds on acoustic propagation in the surf zone. *IEEE Journal of Oceanic Engineering* **26**, 113–124 (2001).

90. Garrett, C., Li, M. & Farmer, D. The Connection between Bubble Size Spectra and Energy Dissipation Rates in the Upper Ocean. *Journal of Physical Oceanography* **30**, 2163–2171 (2000).

91. Wang, D. W., Wijesekera, H. W., Jarosz, E., Teague, W. J. & Pegau, W. S. Turbulent Diffusivity under High Winds from Acoustic Measurements of Bubbles. *Journal of Physical Oceanography* **46**, 1593–1613 (2016).

92. Knudsen, V.O., Alford R.S and Emling, L. W. Underwater Ambient Noise. *Marine Reseatch* **7**, (1948).

93. Wenz, G. M. Acoustic Ambient Noise in the Ocean: Spectra and Sources. *The Journal of the Acoustical Society of America* **34**, 1936–1956 (1962).

94. Farmer, D. M. & Vagle, S. Waveguide propagation of ambient sound in the ocean-surface bubble layer. *The Journal of the Acoustical Society of America* **86**, 1897–1908 (1989).

95. Buckingham, M. J. On Acoustic Transmission in Ocean-Surface Waveguides. *Philosophical Transactions: Physical Sciences and Engineering* **335**, 513–555 (1991).

96. Zhao, Z., D'Asaro, E. A. & Nystuen, J. A. The Sound of Tropical Cyclones. *Journal of Physical Oceanography* **44**, 2763–2778 (2014).

97. Felizardo, F. C. & Melville, W. K. Correlations between Ambient Noise and the Ocean Surface Wave Field. *Journal of Physical Oceanography* **25**, 513–532 (1995).

98. Zhao, B. *et al.* Sensitivity of typhoon modeling to surface waves and rainfall. *Journal of Geophysical Research: Oceans* **122**, 1702–1723 (2017).

99. Vagle, S., McNeil, C. & Steiner, N. Upper ocean bubble measurements from the NE Pacific and estimates of their role in air-sea gas transfer of the weakly soluble gases nitrogen and oxygen. *Journal of Geophysical Research* **115**, C12054 (2010).

100. Cazau, D., Bonnel, J. & Baumgartner, M. Wind Speed Estimation Using Acoustic Underwater Glider in a Near-Shore Marine Environment. *IEEE Transactions on Geoscience and Remote Sensing* **57**, 2097–2106 (2019).

101. Cazau, D., Bonnel, J., Jouma'a, J., le Bras, Y. & Guinet, C. Measuring the Marine Soundscape of the Indian Ocean with Southern Elephant Seals Used as Acoustic Gliders of Opportunity. *Journal of Atmospheric and Oceanic Technology* **34**, 207–223 (2017).

102. Farrell, W. E. *et al.* Wind Sea behind a Cold Front and Deep Ocean Acoustics. *Journal of Physical Oceanography* **46**, 1705–1716 (2016).

103. Cauchy, P., Heywood, K. J., Merchant, N. D., Queste, B. Y. & Testor, P. Wind Speed Measured from Underwater Gliders Using Passive Acoustics. *Journal of Atmospheric and Oceanic Technology* **35**, 2305–2321 (2018).